Localization of Quaternary slip rates in an active rift in 10(5) years: an example from central Greece constrained by U-234-Th-230 coral dates from uplifted paleoshorelines

Journal Article

JOURNAL OF GEOPHYSICAL RESEARCH, VOL. 114, B10406, doi:10.1029/2008JB005818, 2009

Localization of Quaternary slip rates in an active rift in 10^5 years: An example from central Greece constrained by ^{234}U-^{230}Th coral dates from uplifted paleoshorelines

G. P. Roberts,[1] S. L. Houghton,[1] C. Underwood,[1] I. Papanikolaou,[1] P. A. Cowie,[2] P. van Calsteren,[3] T. Wigley,[1] F. J. Cooper,[4,5] and J. M. McArthur[1]

Received 20 May 2008; revised 17 November 2008; accepted 26 June 2009; published 31 October 2009.

[1] Mapping, dating, and modeling of paleoshorelines uplifted in the footwall of the 1981 Gulf of Corinth earthquake fault, Greece (Ms 6.9–6.7), are used to assess its slip rate history relative to other normal faults in the area and study strain localization. The ^{234}U-^{230}Th coral ages from *Cladocora caespitosa* date uplifted shoreface sediments, and paleoshorelines from glacioeustatic sea level highstands at 76, (possibly) 100, 125, 175, 200, 216, 240, and 340 ka. Uplifted Quaternary and Holocene paleoshorelines decrease in elevation toward the western tip of the fault, exhibiting larger tilt angles with age, showing that uplift is due to progressive fault slip. Since 125 ka, uplift rates varied from 0.25 to 0.52 mm/yr over a distance of 5 km away from the fault tip. Tilting was also occurring prior to 125 ka, but uplift rates were lower because the 125 ka paleoshoreline is at 77% of the elevation of the 240 ka paleoshoreline despite being nearly half its age. Comparison of paleoshoreline elevations and sedimentology with the Quaternary sea level curve shows that slip rates increased by a factor of 3.2 ± 0.2 at 175 ± 75 ka, synchronous with cessation of activity on a neighboring normal fault at 382–112 ka. We suggest that the rapid localization of up to 10–15 mm/yr of extension into the narrow gulf (~30 km wide) resulted from synchronous fault activity on neighboring faults followed by localization rather than sequential faulting, with consequences for the mechanism controlling localization of extension.

Citation: Roberts, G. P., S. L. Houghton, C. Underwood, I. Papanikolaou, P. A. Cowie, P. van Calsteren, T. Wigley, F. J. Cooper, and J. M. McArthur (2009), Localization of Quaternary slip rates in an active rift in 10^5 years: An example from central Greece constrained by ^{234}U-^{230}Th coral dates from uplifted paleoshorelines, *J. Geophys. Res.*, *114*, B10406, doi:10.1029/2008JB005818.

1. Introduction

[2] Constructive plate boundaries evolve from areas of distributed normal faulting in continental rifts yet the timescale over which strain localizes onto the plate boundary is known for few examples because of limitations in dating synrift stratigraphy [e.g., *Cowie et al.*, 2005]. Central Greece is among the most rapidly extending portions of the Earth's continental crust, with 10–15 mm/yr of north-south extension localized within a <30 km wide approximately E–W zone associated with the Gulf of Corinth (Figure 1a) [*Billiris et al.*, 1991; *Davies et al.*, 1997; *Clarke et al.*, 1998; *Briole et al.*, 2000]. When and how extension became localized in its present position is not well known because of the lack of detailed fault-specific displacement histories with good age control. This paper presents ^{234}U-^{230}Th coral dates for paleoshorelines formed during localization of faulting that show how Quaternary slip rates changed through time on a 10^5 timescale. This allows us to discuss the mechanisms responsible for the localization.

[3] At the present day, coastal uplift occurs within the footwalls of high slip rate active north dipping normal faults (~1–10 mm/yr [*Cowie and Roberts*, 2001]), close to the southern shores of the Gulf of Corinth, evidenced by uplifted Quaternary and Holocene paleoshorelines [*Keraudren and Sorel*, 1987; *Armijo et al.*, 1996; *Dia et al.*, 1997; *Morewood and Roberts*, 1999; *De Martini et al.*, 2004; *McNeill and Collier*, 2004; *Leeder et al.*, 2003, 2005; *Cooper et al.*, 2007]. These faults have been ruptured by seven >Ms 6.0 normal faulting earthquakes since 1909 A.D., including two large normal faulting earthquakes in the eastern gulf (February 1981; Ms 6.9, 6.7) [*Ambraseys and Jackson*, 1990]. These faults have clear geomorphic expressions and display evidence for repeated offsets in the upper Quaternary and Holocene. Of interest here, is that these active faults have uplifted other normal faults located to the south of the gulf,

[1]Department of Earth and Planetary Sciences, Birkbeck College, University of London, London, UK.
[2]Institute of Earth Science, School of GeoSciences, Edinburgh University, Edinburgh, UK.
[3]Uranium Series Facility, Department of Earth Sciences, Open University, Milton Keynes, UK.
[4]Departmet of Earth Sciences, University of Southern California, Los Angeles, California, USA.
[5]Now at School of Earth and Space Exploration, Arizona State University, Tempe, Arizona, USA.

0148-0227/09/2008JB005818$09.00

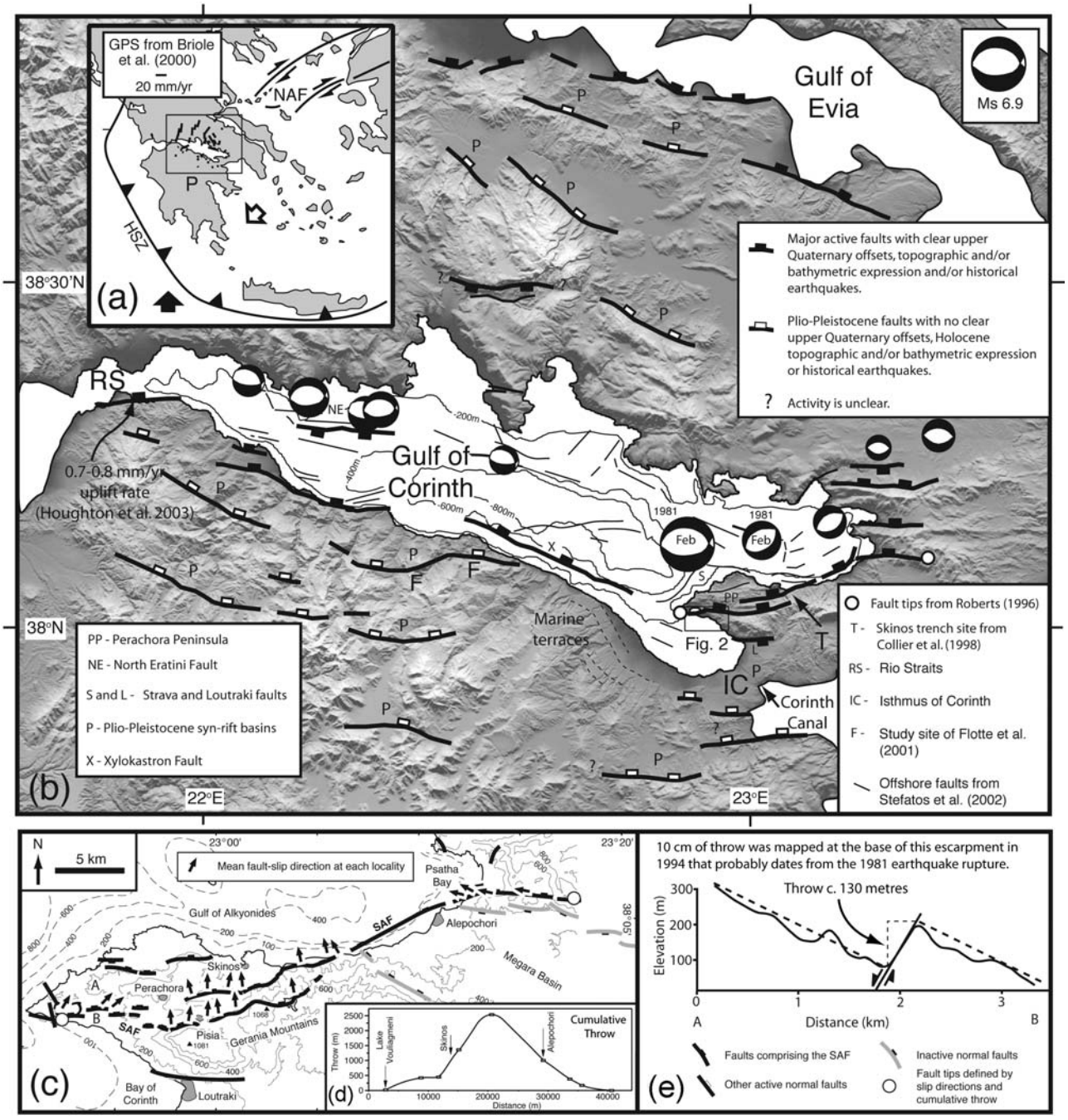

Figure 1. Location map for the Gulf of Corinth, Greece. (a) GPS velocities in a fixed Peloponese (P) reference frame after *Briole et al.* [2000]. NAF, North Anatolian Fault; HSZ, Hellenic Subduction Zone. The white arrow shows the motion of the Aegean. The black arrows show the motion of Africa. Box locates Figure 2. (b) SRTM DEM showing the main active faults, and faults that have either ceased activity or have slip rates that are too low to produce a clear geomorphic expression of Holocene slip or large magnitude (Ms > 5.8) historical earthquakes. Bathymetry and offshore faults are shown only for the Gulf of Corinth. Focal mechanisms are modified from *Ambraseys and Jackson* [1990] for large magnitude earthquakes (Ms > 6.0) since 1909 A.D. The two onshore faults immediately to the south of the two February 1981 focal mechanisms ruptured in these earthquakes [*Jackson et al.*, 1982]. (c) Detailed map of the fault system that ruptured in the 1981 earthquakes (modified from *Morewood and Roberts* [2002]) and a throw profile. (d) Cumulative throw. (e) Topographic profile from SRTM data across the fault along transect A–B (located in Figure 1c) located 2 km east of Lake Vouliagmeni. We interpret this to show a south dipping topographic surface that has been offset by a north dipping fault with a throw of ~130 m in this location (compare with *Turner et al.* [2008]). The base of this escarpment was ruptured in 1981, confirmed by field observations in 1994 by the authors of a surface rupture.

but the age relationships between them are poorly known. These uplifted faults are either no longer active or have slip rates that are too low to have produced clear geomorphic signatures of Holocene fault slip or large magnitude (>Ms 6.0) historical earthquakes [*Armijo et al.*, 1996; *Jackson*, 1999]. However, they control the thicknesses and facies of Plio-Pleistocene sediments and were active in this time window [*Ori*, 1989; *Malartre et al.*, 2004]. It is unclear when and how extension migrated between the uplifted faults and the presently active faults bounding the coast.

[4] A similar pattern of active normal faults uplifting less active/inactive normal faults is also evident for the Gulf of Evia, located north of the Gulf of Corinth [*Roberts and Jackson*, 1991] (Figure 1). Active north dipping normal faults close to the southern coast of the Gulf of Evia have uplifted normal faults located south of the Gulf of Evia that control the facies and thicknesses of Plio-Pleistocene sediments [*Roberts and Jackson*, 1991]. Overall, active faults in the Gulf of Corinth are located between two zones containing normal faults whose activity was most prevalent during the Plio-Pleistocene. It is not clear how extension on these Plio-Pleistocene faults was transformed into the present-day extension localized on active faults in the Gulf of Corinth and Gulf of Evia.

[5] One possibility is that faulting stepped to the north in both the gulfs of Corinth and Evia [*Vita-Finzi and King*, 1985; *Jackson*, 1999; *Goldsworthy and Jackson*, 2001; *Goldsworthy et al.*, 2002]. In this scenario, presently active faults developed to accommodate the ongoing extension when slip on faults to the south of each gulf ceased. Such sequential fault activity, at least for the Gulf of Corinth, has been suggested to develop either (1) as the faults react to block rotations within a regional velocity field that is controlled by larger-scale effects such as buoyancy forces and movements of subducted slabs [*Goldsworthy and Jackson*, 2001] or (2) where the fault system reacts to the migration at depth of the transition from a flat to steeply dipping subduction [*Leeder et al.*, 2003].

[6] A second possibility is that all the faults in Figure 1b were active synchronously in the Pliocene and lower Pleistocene. Displacement then localized, with the majority of extension concentrated within the gulfs of Corinth and Evia in the late Pleistocene. In this scenario, extension localized within, rather than to the north of the area of Plio-Pleistocene extension. Such synchronous fault activity followed by localization in the Gulf of Corinth, has been suggested to develop (1) owing to elastic interaction between structures during growth and propagation of the North Anatolian Fault [*Armijo et al.*, 1996], (2) where loads associated with erosion, sedimentation and influx of the sea induced by a climatic change at ~0.9 Ma caused deformation to localize at the present position of the Gulf of Corinth [*Westaway*, 1996, 1998, 2002, 2007], or (3) where rift localization is driven by growth and interaction between normal faults [*Cowie and Roberts*, 2001], with coupling between the development of brittle normal faults in the near surface and the thermal evolution of a rheologically layered lithosphere, with the balance of the two coupled effects being a function of the regional extension rate [*Cowie et al.*, 2005].

[7] We argue that the response times associated with the deformation processes described above will differ and that this may be the key for discriminating between them. This paper provides data on the timescale over which fault geometries evolved in the Gulf of Corinth and uses this information to assess the underlying causes of displacement localization.

[8] We present new mapping and dating of Quaternary paleoshorelines uplifted in the footwall of the 1981 earthquake fault in the eastern Gulf of Corinth and review evidence for uplift of Holocene paleoshorelines. These data constrain the 10^3–10^6 year history of slip on this fault (Figures 1 and 2). We present (1) maps and profiles of the inner edges of marine terrace deposits and wave-cut platforms that we interpret as paleoshoreline indicators (Figures 2, 3, and 4 and auxiliary material Table S1), (2) ^{234}U-^{230}Th dates on corals found within paleoshoreface deposits that can be mapped into paleoshoreline locations, constraining paleoshorelines ages (Table 1 and Figures 2, 3, and 4), (3) ^{234}U-^{230}Th dates on paleoshoreface deposits that cannot be mapped into paleoshoreline locations but are intercalated with subaerial deposits revealing a history of transgressions and regressions that we relate to the fault-related uplift and the Quaternary sea level curve (Table 1 and Figures 4 and 5), and (4) calculations of uplift rates that explain the mapped and dated paleoshorelines and identify the ages of other undated but mapped shorelines through comparison with the Quaternary sea level curve (Figures 6, 7, and S1 and Table S2).[1] We integrate these observations, dates and calculations to constrain the slip rate history of the 1981 earthquake fault, comparing it to the slip histories of neighboring faults, in order to discuss the temporal and spatial pattern of structural evolution of the Gulf of Corinth (Figures 8 and 9).

2. Previous Work

[9] The 1981 Gulf of Corinth earthquake sequence (24–25 February and 4 March 1981; Ms 6.7, 6.4, 6.2 [*Jackson et al.*, 1982]) provoked many studies of the extension in the Gulf of Corinth. The seismicity, geodesy, active faulting, stratigraphy and uplift/subsidence have been studied in detail (seismicity by *Ambraseys and Jackson* [1990], *Abercrombie et al.* [1995], *Pantosti et al.* [1996], and *Collier et al.* [1998]; geodesy by *Billiris et al.* [1991], *Davies et al.* [1997], *Clarke et al.* [1998], and *Briole et al.* [2000]; active faulting by *Roberts and Jackson* [1991], *Taymaz et al.* [1991], *de Boer* [1992], *Doutsos and Poulimenos* [1992], *Armijo et al.* [1996], *Hubert et al.* [1996], *Roberts* [1996a, 1996b], *Morewood and Roberts* [1999, 2001], *Westaway* [2002], *Goldsworthy et al.* [2002], *Stefatos et al.* [2002], *Leeder et al.* [2003, 2005], and *McNeill et al.* [2005]; stratigraphy by *Higgs* [1988], *Collier et al.* [2000], and *Leeder et al.* [2003]; and uplift/subsidence by *Vita-Finzi and King* [1985], *Collier et al.* [1992], *Pirazzoli et al.* [1994], *Roberts and Stewart* [1994], *Stewart and Vita-Finzi* [1996], *Dia et al.* [1997], *Morewood and Roberts* [1999], *Kershaw and Guo* [2001], *Leeder et al.* [2003], *Cooper et al.* [2007], and *Sakellariou et al.* [2007]). However, this paper highlights the fact that debate continues concerning the timing of

[1] Auxiliary materials are available in the HTML. doi:10.1029/2008JB005818.

Table 1. The ^{234}U-^{230}Th Chemical and Isotopic Data for *Cladocora caespitosa* Coral[a]

Sample Name	Sample Number	Wall or Septa of Corallites	Age (ka)	Age Plus Error	Age Minus Error	UTM Longitude	UTM Latitude	Sampling Elevation (m)	Total U (Error 2 SE) (ppm)	Total Th (Error 2 SE) (ppb)	($^{230}Th/^{234}U$) (Error 2 SE)	($^{230}Th/^{232}Th$) (Error 2 SE)	$\delta^{234}U$ (0)	$\delta^{234}U$ (T)	Assigned Highstand
P1SR1aw	1[b]	Wall	76.2	1	1	669215	4208612	10	2.720 ± 0.024	3.95 ± 0.36	0.509 ± 0.008	1243 ± 30	148	184	76 ka
W20	2[b]	Wall	125	4.2	4.1	668447	4209303	25	2.629 ± 0.022	1.88 ± 0.17	0.694 ± 0.012	3410 ± 85	135	191	125 ka
P1SS2w	3[b]	Wall	240	5.7	5.4	669400	4208892	85	2.424 ± 0.016	1.92 ± 0.17	0.918 ± 0.011	4084 ± 81	137	270	240 ka
P1SS2w up	4[b]	Wall	248	7.2	6.7	669400	4208892	85	2.476 ± 0.021	3.11 ± q0.28	0.932 ± 0.013	2679 ± 58	165	333	240 ka
P1ST2w	5[c]	Wall	> 350			669397	4208877	78	2.421 ± 0.028	3.13 ± 0.28	1.092 ± 0.014	2981 ± 61	-	-	340 ka?
P1ST2w	5[c]	Wall	> 350			669397	4208877	78	2.708 ± 0.024	3.36 ± 0.30	1.103 ± 0.020	3150 ± 81	-	-	340 ka?
P1S1bw	6[b]	Wall	178	6.4	6.4	669313	4208426	9.5	2.577 ± 0.026	1.28 ± 0.11	0.825 ± 0.011	5947 ± 126	145	240	175 ka
P1S2bw	7[b]	Wall	201	3.4	3.3	669313	4208426	9	2.901 ± 0.026	2.70 ± 0.24	0.875 ± 0.010	3512 ± 67	203	359	200 ka
P1S4w	8[b]	Wall	211	4.3	4.1	669313	4208426	8.5	2.601 ± 0.030	3.12 ± 0.40	0.884 ± 0.010	2645 ± 73	161	291	216 ka
P1S/1w	9[b]	Wall	337	37	26	669313	4208426	6.5	2.300 ± 0.121	1.91 ± 0.18	0.994 ± 0.016	4172 ± 91	140	363	340 ka
P1S/2w	10[c]	Wall	162	2.3	2.2	669313	4208426		2.616 ± 0.023	3.74 ± 0.35	0.797 ± 0.009	2036 ± 41	191	301	175 ka
P1S5w	11[c]	Wall	161	4.4	4.4	669313	4208426		2.828 ± 0.024	3.64 ± 0.32	0.791 ± 0.009	2181 ± 30	147	232	175 ka
P1S/3w	12[d]	Wall	138	2.2	2	669313	4208426		2.331 ± 0.037	6.60 ± 0.59	0.731 ± 0.010	901 ± 20	131	193	Unclear
P1S/2s	13[d,e]	Septa	227	4.9	4.6	669313	4208426		2.863 ± 0.023	5.72 ± 0.53	0.910 ± 0.011	1652 ± 34	179	340	Unclear
P1/S1s	14[d]	Septa	312	12	11	669313	4208426		2.744 ± 0.015	6.45 ± 0.61	0.981 ± 0.013	1476 ± 32	149	358	Unclear
P1/S1s	15[d]	Septa	308	10	9.6	669313	4208426		2.744 ± 0.015	6.45 ± 0.61	0.979 ± 0.012	1472 ± 30	149	355	Unclear
P1/S1s	16[d]	Septa	279	8.9	8.2	669313	4208426		2.744 ± 0.015	6.45 ± 0.61	0.958 ± 0.013	1441 ± 32	149	327	Unclear
P13w	17[c]	Wall	356	50	32	668227	4209462		2.503 ± 0.15	3.83 ± 0.38	1.007 ± 0.017	2358 ± 53	157	429	340 ka
PB2w	18[b]	Wall	156	2	1.9	665429	4210205	33	3.112 ± 0.024	2.25 ± 0.21	0.788 ± 0.008	4103 ± 79	231	358	125 ka?
PB4w	19[b]	Wall	122	1.2	1.2	665429	4210205	33	2.631 ± 0.012	1.75 ± 0.16	0.688 ± 0.007	3582 ± 68	146	206	125 ka
PB4w	20[b,e]	Wall	139	2.4	2.4	665429	4210205	33	2.884 ± 0.015	4.82 ± 0.45	0.737 ± 0.012	1551 ± 39	144	213	125 ka
PB7w	21[b,e]	Wall	154	1.9	1.8	665429	4210205	33	3.328 ± 0.024	1.57 ± 0.15	0.775 ± 0.008	5805 ± 114	158	243	125 ka
PB4s	22[d]	Septa	141	1.7	1.7	665429	4210205	33	3.255 ± 0.022	2.05 ± 0.19	0.742 ± 0.008	4115 ± 81	148	220	Unclear
PB4s	23[d,e]	Septa	152	2.8	2.7	665429	4210205	33	3.255 ± 0.022	1.85 ± 0.17	0.769 ± 0.013	4738 ± 117	148	227	Unclear
PB7s	24[d,e]	Septa	131	1.6	1.6	665429	4210205	33	3.341 ± 0.023	1.26 ± 0.12	0.715 ± 0.009	6490 ± 133	149	216	Unclear
P1/1w	25[f,g]	Wall	116	1.4	1.4	662500	4210750		2.229 ± 0.025	4.82 ± 0.45	0.673 ± 0.009	1181 ± 25	233	323.82	100 ka?
P1/1s	26[d,e]	Septa	141	1.7	1.7	662500	4210750		2.586 ± 0.016	5.62 ± 0.52	0.741 ± 0.008	1205 ± 24	148	221	Unclear
SMC	27[c]	Wall	0.5	0.06	0.06	665911	4213489	0	2.342 ± 0.017	0.69 ± 0.10	0.005 ± 0.001	168 ± 22	151	151	0 ka

[a]We discuss individual samples in Text S1, commenting on the reliability of each date and the field relationships of each sample.
[b]We are confident of the date and field relationship, and we have used the date in our stratigraphic interpretation.
[c]We are confident of the date, but we were unable to assign a stratigraphic interpretation due to unclear field relationships.
[d]We are not confident of the date, although the field relationship in some instances is clear and have not used the date in our interpretation.
[e]A trace of calcite was found in the samples prior to cleaning.
[f]We are not confident of the date but the implied field relationship is discussed.
[g]A trace of gypsum was found in the samples prior to cleaning.

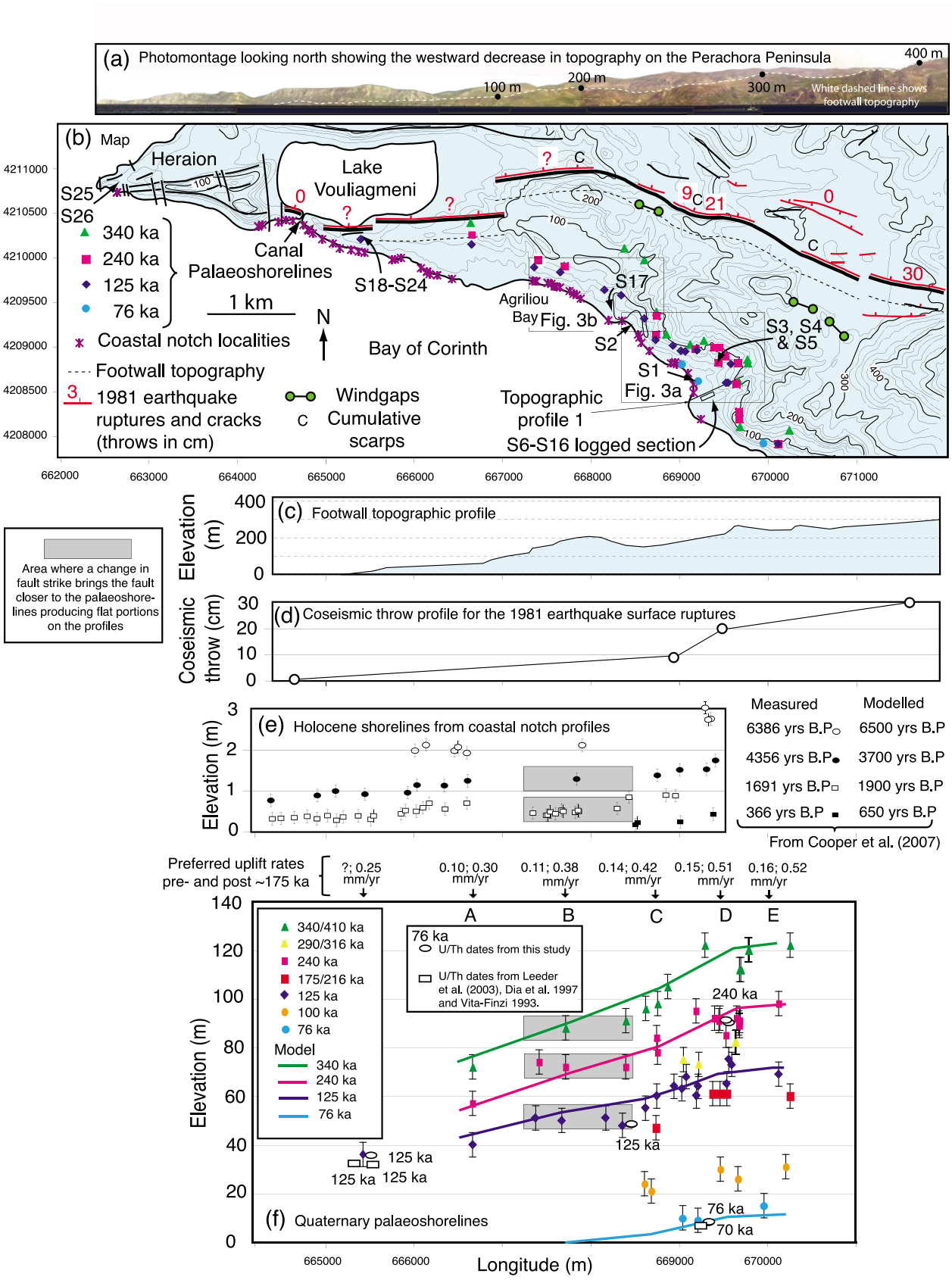
(a) Photomontage looking north showing the westward decrease in topography on the Perachora Peninsula
400 m
200 m
100 m
300 m
White dashed line shows footwall topography
(b) Map
Heraion
Lake Vouliagmeni
S25
S26
340 ka
240 ka
125 ka
76 ka
Canal Palaeoshorelines
S18-S24
1 km
N
Bay of Corinth
Agriliou Bay
Fig. 3b
S17
S2
S1
Fig. 3a
S3, S4 & S5
Topographic profile 1
S6-S16 logged section
Coastal notch localities
Footwall topography
1981 earthquake ruptures and cracks (throws in cm)
Windgaps
Cumulative scarps
4211000
4210500
4210000
4209500
4209000
4208500
4208000
662000
663000
664000
665000
666000
667000
668000
669000
670000
671000
Area where a change in fault strike brings the fault closer to the palaeoshore-lines producing flat portions on the profiles
(c) Footwall topographic profile
Elevation (m)
(d) Coseismic throw profile for the 1981 earthquake surface ruptures
Coseismic throw (cm)
(e) Holocene shorelines from coastal notch profiles
Elevation (m)
Measured
Modelled
6386 yrs B.P
6500 yrs B.P
4356 yrs B.P
3700 yrs B.P
1691 yrs B.P
1900 yrs B.P
366 yrs B.P
650 yrs B.P
From Cooper et al. (2007)
Preferred uplift rates pre- and post ~175 ka
?; 0.25 mm/yr
0.10; 0.30 mm/yr
0.11; 0.38 mm/yr
0.14; 0.42 mm/yr
0.15; 0.51 mm/yr
0.16; 0.52 mm/yr
A
B
C
D
E
340/410 ka
290/316 ka
240 ka
175/216 ka
125 ka
100 ka
76 ka
Model
340 ka
240 ka
125 ka
76 ka
76 ka
U/Th dates from this study
U/Th dates from Leeder et al. (2003), Dia et al. 1997 and Vita-Finzi 1993.
240 ka
125 ka
125 ka
125 ka
125 ka
76 ka
70 ka
(f) Quaternary palaeoshorelines
Elevation (m)
Longitude (m)
665000
666000
669000
670000

Figure 2

initiation of slip on individual faults (see section 1), and the spatial and temporal patterns of uplift related to this fault evolution. For example, marine terraces around the Gulf of Corinth have been interpreted as indicating a constant uplift rate through time [*Armijo et al.*, 1996; *Morewood and Roberts*, 1999], or an increasing uplift rate [*Westaway*, 2002, 2007]. This has led to debate on the timescale and mechanism responsible for the deformation. Also, some authors suggest that marine terraces on the Perachora Peninsula in the eastern gulf are tilted [*Morewood and Roberts*, 1999; *Cooper et al.*, 2007], whereas others suggest spatially uniform uplift [*Leeder et al.*, 2003, 2005]. Our detailed mapping and dating of paleoshorelines helps to differentiate between these hypotheses and establish the temporal and spatial patterns of uplift.

[10] Specifically, we study the fault that ruptured in the 1981 earthquakes (Figures 1 and 2). *Morewood and Roberts* [1999] mapped marine terraces along the 1981 earthquake fault eastward from a site with ^{234}U-^{230}Th coral dates that indicate a paleoshoreline from 125 ka [*Vita-Finzi*, 1993]. They suggested that uplift increased eastward along the coast for at least ~5 km from the canal entrance to Lake Vouliagmeni (Figure 2). This change in uplift was suggested to correlate both with the general eastward increase in footwall topography, and throw along the fault that ruptured in the 1981 earthquakes, and with the eastward increase in coseismic throws across surface ruptures for this earthquake reported by *Jackson et al.* [1982] and *Bornovas et al.* [1984] (Figures 2c and 2d). Thus, uplift was suggested to record the eastward increase in cumulative slip from repeated coseismic displacements on this fault in the late Quaternary and Holocene. This uplift progressively altered the drainage to form wind gaps (Figure 2b) and ultimately form the internal drainage of Lake Vouliagmeni (now breached by human excavation of a canal). Repeated displacements in the late Quaternary and Holocene are also evidenced by faulted carbonate buildups that underlie a coral-bearing bioclastic sand dated to 125 ka [*Vita-Finzi*, 1993; *Morewood and Roberts*, 1997; *Portman et al.*, 2005] and cumulative scarps formed where Holocene sedimentation has not kept pace with fault slip [*Morewood and Roberts*, 1999]. *Cooper et al.* [2007] support these interpretations, presenting detailed elevation profiles of Holocene paleoshorelines (coastal notches) in the footwall of the 1981 earthquake fault (Figures 2b and 2e). These coastal notches increase in elevation to the east, indicating an eastward increase in uplift rate. *Cooper et al.* [2007] correlated notch ages with radiometric determinations from *Pirazzoli et al.* [1994], by extrapolating uplift rates from the 125 ka terrace dated by *Vita-Finzi* [1993] and *Leeder et al.* [2003] to explain the measured elevations of the Holocene paleoshorelines. In contrast, *Leeder et al.* [2003, paragraph 6] found "little evidence for regionally significant late Quaternary faulting," with the "elevation of both Holocene and upper Quaternary shoreline features showing no systematic changes" [see also *Leeder et al.*, 2005, p. 555]. They suggested uplift is uniform across the region shown in Figure 2. *Leeder et al.* [2003] did not present detailed Holocene notch elevation profiles, or mark the inner edges of upper Quaternary paleoshorelines on maps with topographic contours, so it is difficult to evaluate their findings. *Leeder et al.* [2005] did present inner edge locations on a map with topographic contours every 20 m but provided no new radiometric ages to support their terrace elevation map at the actual locations close to Agriliou Bay (Figure 2), which they use to suggest uniform uplift. However, in support of *Leeder et al.* [2003, 2005], *Morewood and Roberts* [1999] lacked radiometric dates for paleoshorelines older than 125 ka. They mapped on low-resolution 1:25,000 topographic base maps with 20 m contour intervals, while *Leeder et al.* [2003] used 1:5000 maps and "altimetric determinations" and provided new U/Th dates for corals in the 125 ka deposits. We have not been able to discriminate between these varied uplift possibilities using other coral dates provided by *Dia et al.* [1997] for the Perachora Peninsula. This is because we were unable to determine the exact locations of the corals they sampled or the associated paleoshoreline inner edges from their paper.

[11] Thus, in order to address the debate on "uniform" versus "eastward increasing" paleoshoreline elevations, and address the wider issue of "synchronous" versus "sequential" faulting, this paper presents mapping on 1:5000 base maps (Figures 2, 3, and S2 and Table S1) with elevations checked with barometric altimeters and GPS, together with new radiometric determinations of paleoshoreline ages (Table 1), including age determinations for paleoshorelines older and younger than 125 ka. The work has showed that study of the sedimentology of paleoshoreface sediments associated with the paleoshorelines improves the details of the uplift rate determination; in section 3, we describe these

Figure 2. Paleoshorelines, topography, and active faulting on the Perachora Peninsula with UTM coordinates. Figures 2a–2f are shown in their correct positions with regard to longitude. (a) Photo montage looking north showing the topographic decrease from east to west in the footwall of the fault that ruptured in the 1981 Gulf of Corinth earthquakes. (b) Map of the active faults that ruptured in 1981. Coseismic throws decreased from east to west. The simplified locations and elevations of paleoshorelines mapped in this study are shown. Boxes locate more detailed maps in Figures 3a, 3b, and S2. "S" numbers locate sample sites. (c) and (d) Decrease in topography and coseismic throw in 1981 from east to west. (e) Decrease in elevation from east to west of Holocene paleoshorelines (coastal notches). Numbers refer to measured ages and modeled ages [*Cooper et al.*, 2007]. Notches to the west of Lake Vouliagmeni have varied elevations due to Holocene slip on faults with north-south strikes [*Kershaw and Guo*, 2001], so we do not attempt to correlate notch elevations across this area. (f) Profiles showing the east to west decrease in elevation of upper Quaternary paleoshorelines described in this study. Open symbols show ^{234}U-^{230}Th coral dates that constrain the ages of the paleoshorelines. We are uncertain of the exact location of the 70 ka date from *Dia et al.* [1997]. Numbers refer to the implied uplift rates from model fits before and after 175 ka derived from the calculations in this study (see text for explanation and Figure 7). A–E are profiles referred to in Figure 7.

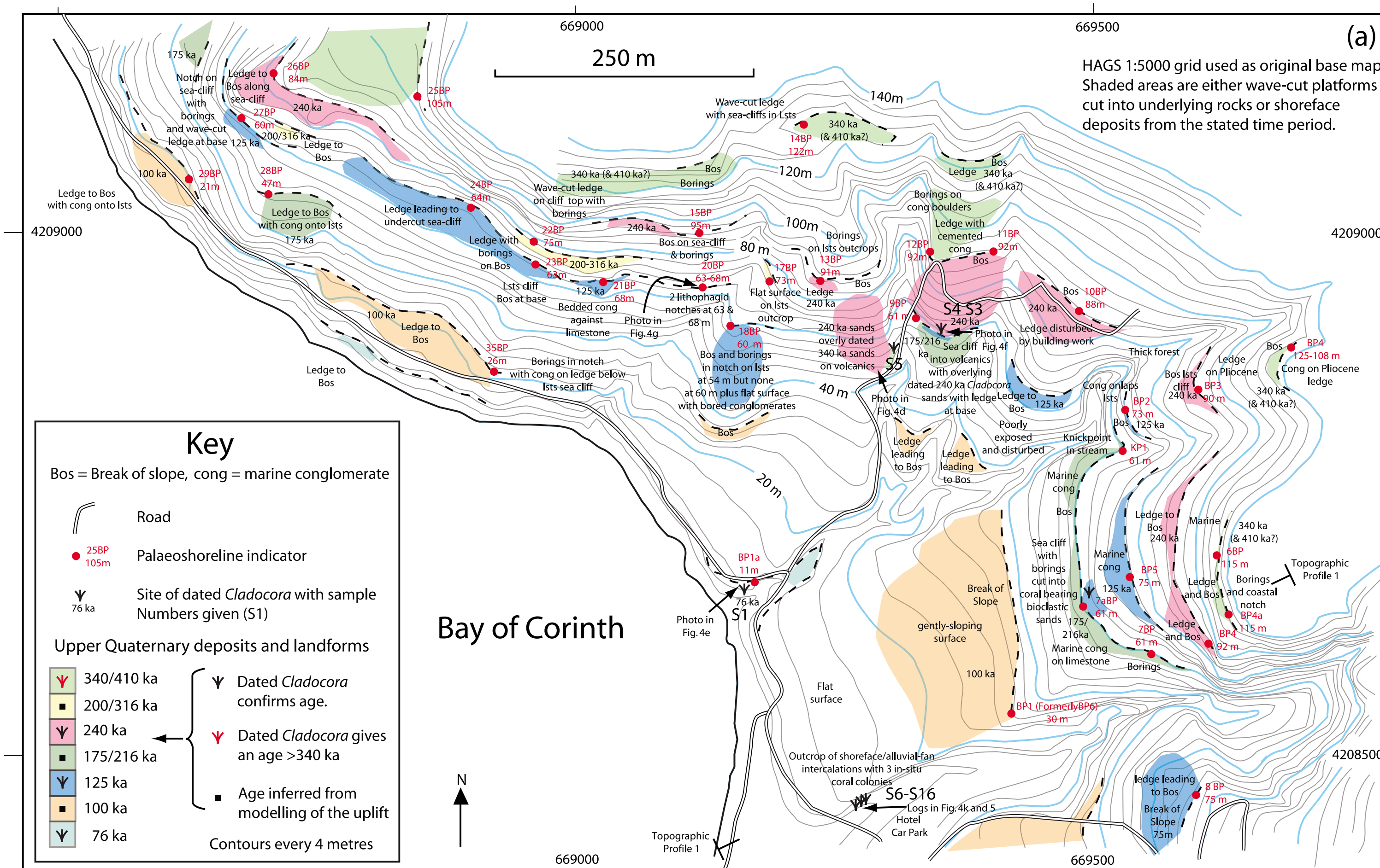

Figure 3. Detailed paleoshoreline maps (a) from the eastern part of the mapped area and (b) from the central part of the mapped area (extracted from a larger map in Figure S2). Topographic base map is redrawn from the Hellenic Army Geographic Service (HAGS) with a UTM grid added. Shaded areas show the locations of wave-cut platforms and deposits related to individual paleoshorelines. The inner edges (back points; BP) of these features are characterized by paleoshoreline indicators such as paleosea cliffs, coastal notches, and marine to fluvial sedimentary facies transitions. Brief descriptions of these paleoshoreline indicators are given for each inner edge. Geographic coordinates of each inner edge are given in Table S1. The ages of these paleoshorelines were derived from ^{234}U-^{230}Th coral dates in the first instance, followed, in the case of paleoshorelines with no corals dates, by calculations that predict the height of known sea level highstands given uplift rates implied by paleoshorelines with coral dates (see text for explanation). Locations of dated *Cladocora* corals are indicated. "Cong" indicates conglomerates; "Bos" indicates break of slope; lsts indicates limestones.

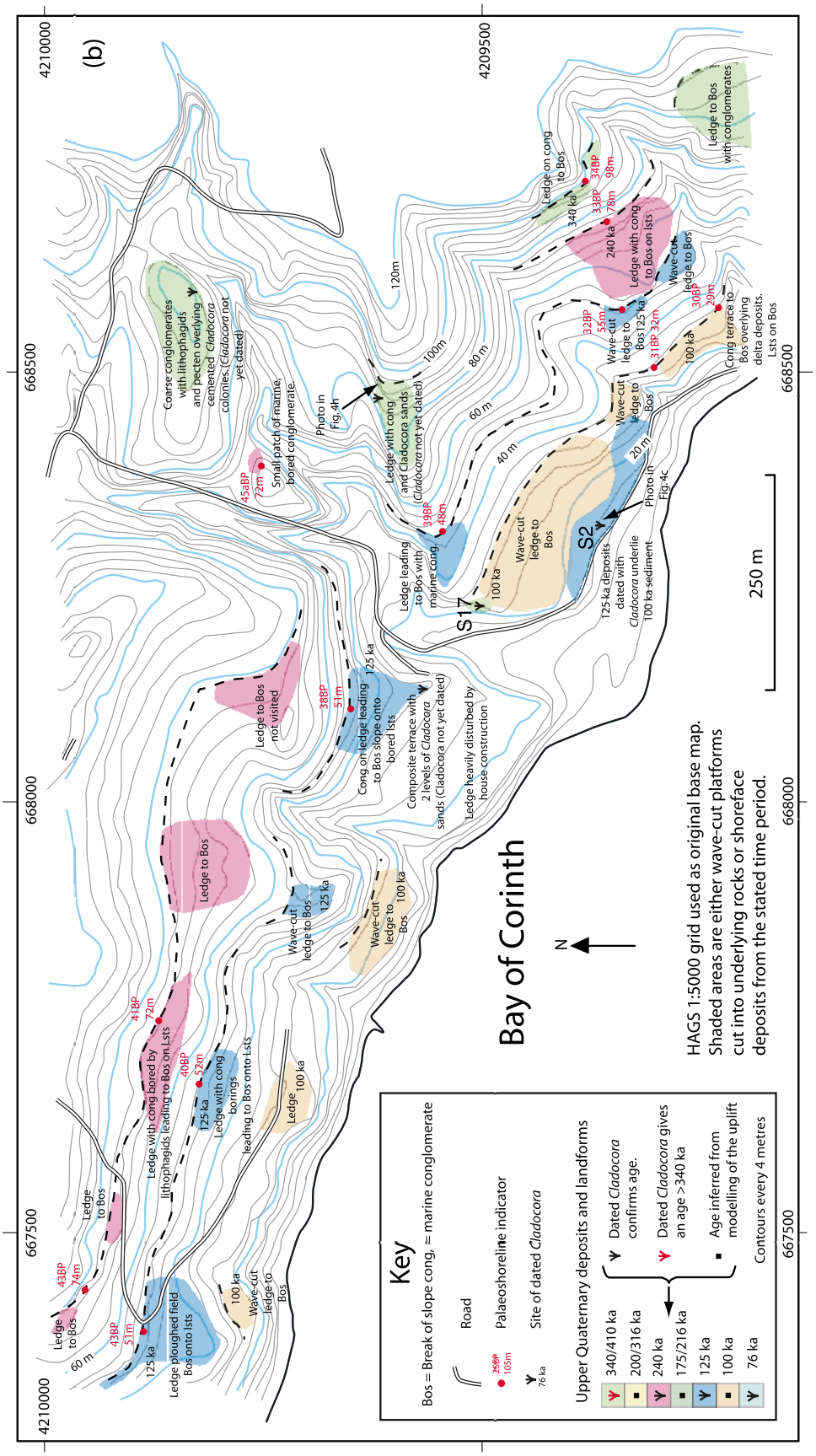

Figure 3. (continued)

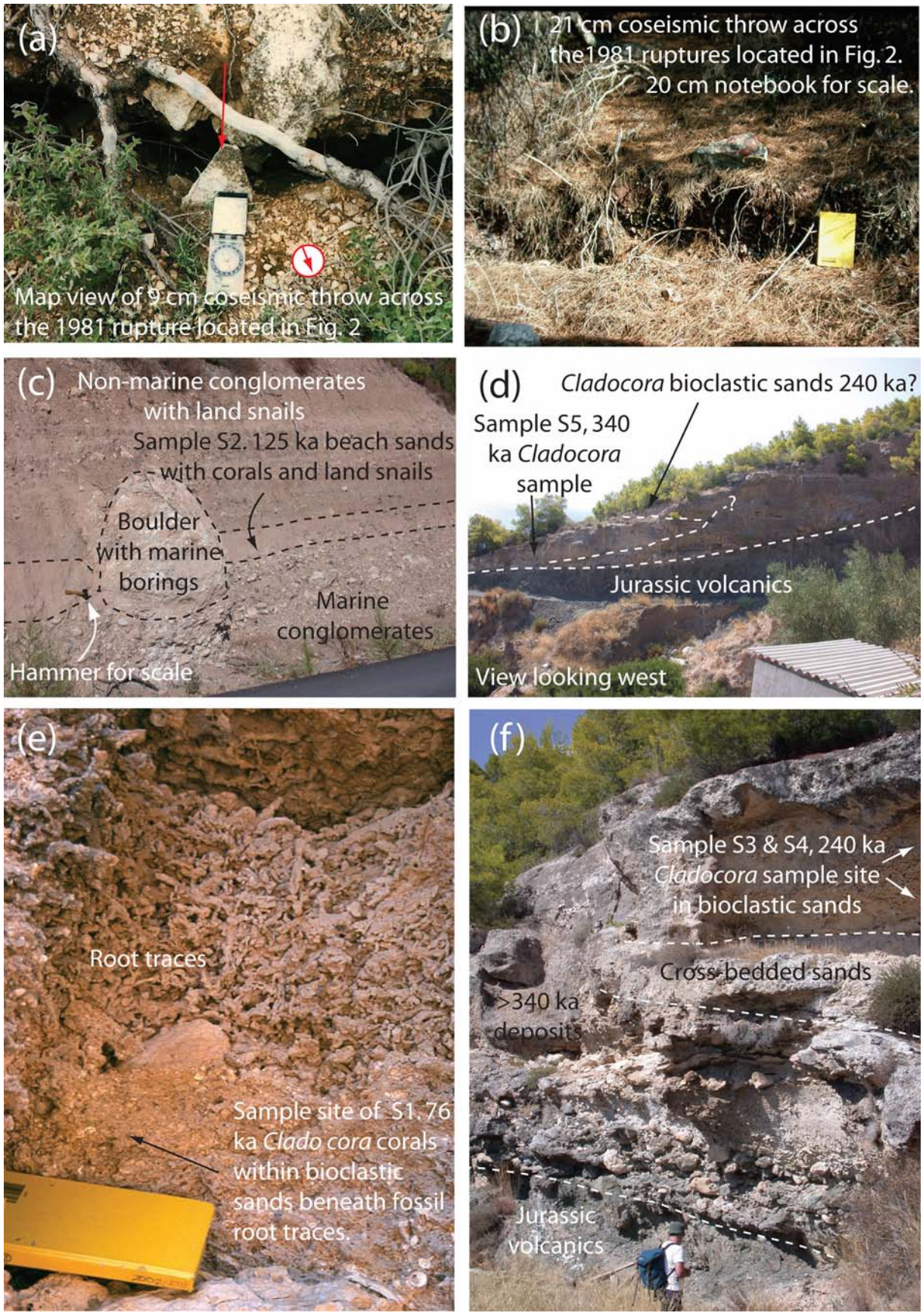
(a)
Map view of 9 cm coseismic throw across the 1981 rupture located in Fig. 2
(b)
21 cm coseismic throw across the1981 ruptures located in Fig. 2.
20 cm notebook for scale.
(c)
Non-marine conglomerates with land snails
Sample S2. 125 ka beach sands with corals and land snails
Boulder with marine borings
Marine conglomerates
Hammer for scale
(d)
Cladocora bioclastic sands 240 ka?
Sample S5, 340 ka Cladocora sample
Jurassic volcanics
View looking west
(e)
Root traces
Sample site of S1. 76 ka Clado cora corals within bioclastic sands beneath fossil root traces.
(f)
Sample S3 & S4, 240 ka Cladocora sample site in bioclastic sands
Cross-bedded sands
>340 ka deposits
Jurassic volcanics

Figure 4

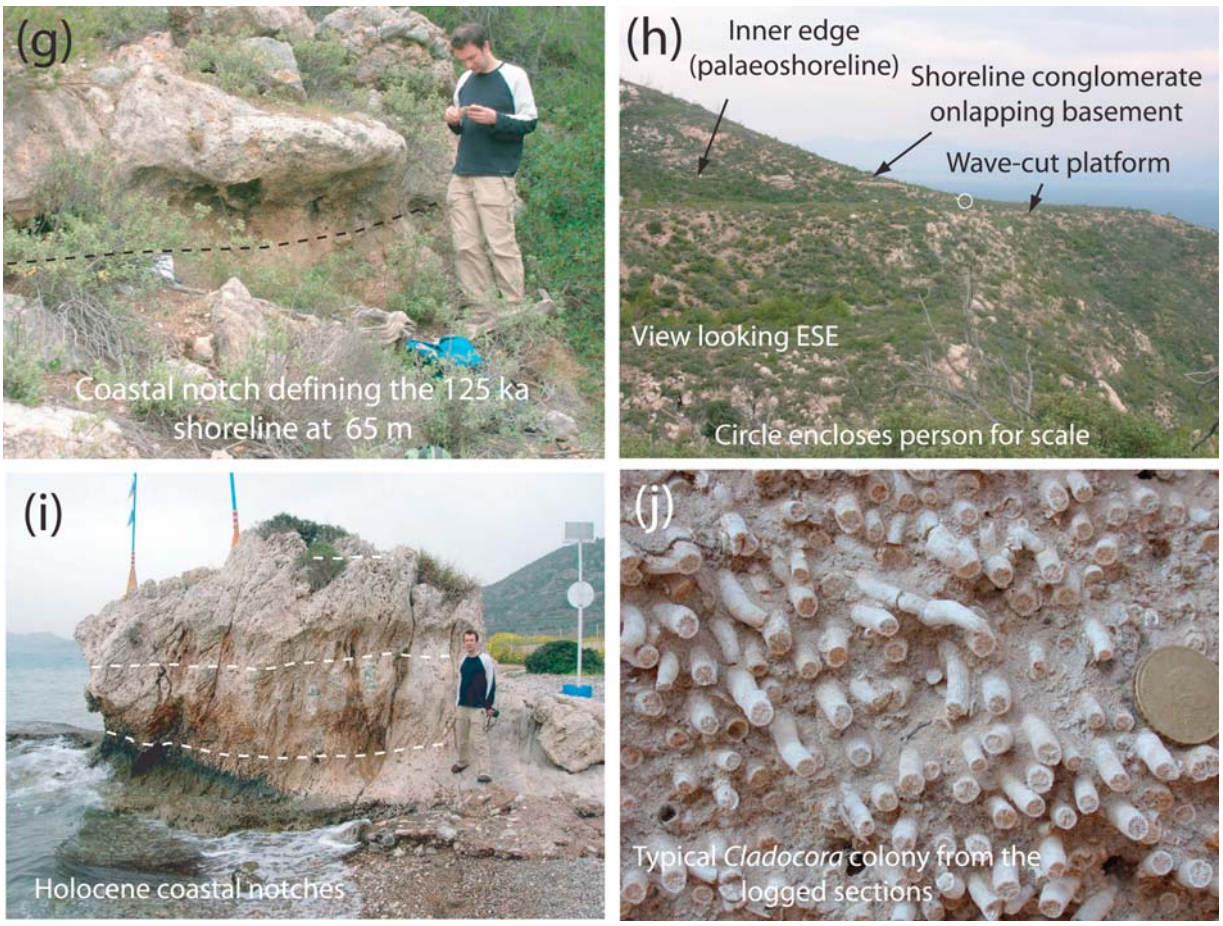

Figure 4. (continued)

sediments in detail before discussing the paleoshoreline elevations.

3. Quaternary Paleoshorelines and Associated Paleoshoreface Sediments

3.1. Characteristics of Paleoshorelines, Wave-Cut Platforms, and Associated Sediments

[12] The paleoshorelines we studied are characterized by wave-cut platforms or shoreface sediments that can be mapped into coastal notches at the bases of paleosea cliffs. In places shoreface sediments are intercalated with subaerial calcretes and alluvial fan sediments. We describe these features in more detail below (Figures 4 and 5) and their locations are given precisely on detailed maps (Figures 3 and S2 and Table S1).

3.2. Wave-Cut Platforms

[13] Wave-cut platforms are erosional surfaces cut by wave action within a few meters of sea level. Uplifted wave-cut platforms in our study area cover areas of a few tens of meters or less because the overall slope on the south coast is relatively steep where the bedrock is relatively resistant to erosion (Figures 2 and 4h). Wave-cut platforms dip at a few degrees or less and terminate updip and inland into breaks of slope that we interpret as fossil sea cliffs (see

Figure 4. (a and b) Photos showing coseismic throws along the 1981 earthquake surface ruptures that demonstrate active faulting in the study area (compare with *Turner et al.* [2008]). Figure 4a shows a map view of the ruptures, photographed in 2001, where the slip vector indicated by the arrow is recorded by displacement of a triangular clast of rock. The slip vector is 13 cm of displacement with a plunge of 45° toward 025° at UTM coordinate 0668832 4210668; the throw is thus 9 cm. The red arrow in a circle shows north as recorded on the compass. Figure 4b shows a location with 21 cm throw across a rupture in alluvium, ~300–400 m to the east of Figure 4a photographed in 1994; a forest fire and subsequent vegetation clearance by a farmer using an agricultural vehicle has since obscured or destroyed the location of this part of the rupture. (c–f) Sample sites for 76, 125, 240, and >340 ka *Cladocora* corals constraining paleoshorelines. (g and h) Typical paleoshoreline indicators such as bored coastal notches and wave-cut platforms leading updip to breaks of slope. (i) Holocene paleoshorelines with dashed lines showing approximate positions of former sea level (see *Cooper et al.* [2007] for more detail). The highest notch with *Lithophaga* is at ~3 m, not 1.5 m as suggested by *Turner et al.* [2008]. (j) A typical in situ *Cladocora* colony. (k–t) Logs and photographs of typical shoreface/alluvial sediments. Photographs and logs are located in Figure 3.

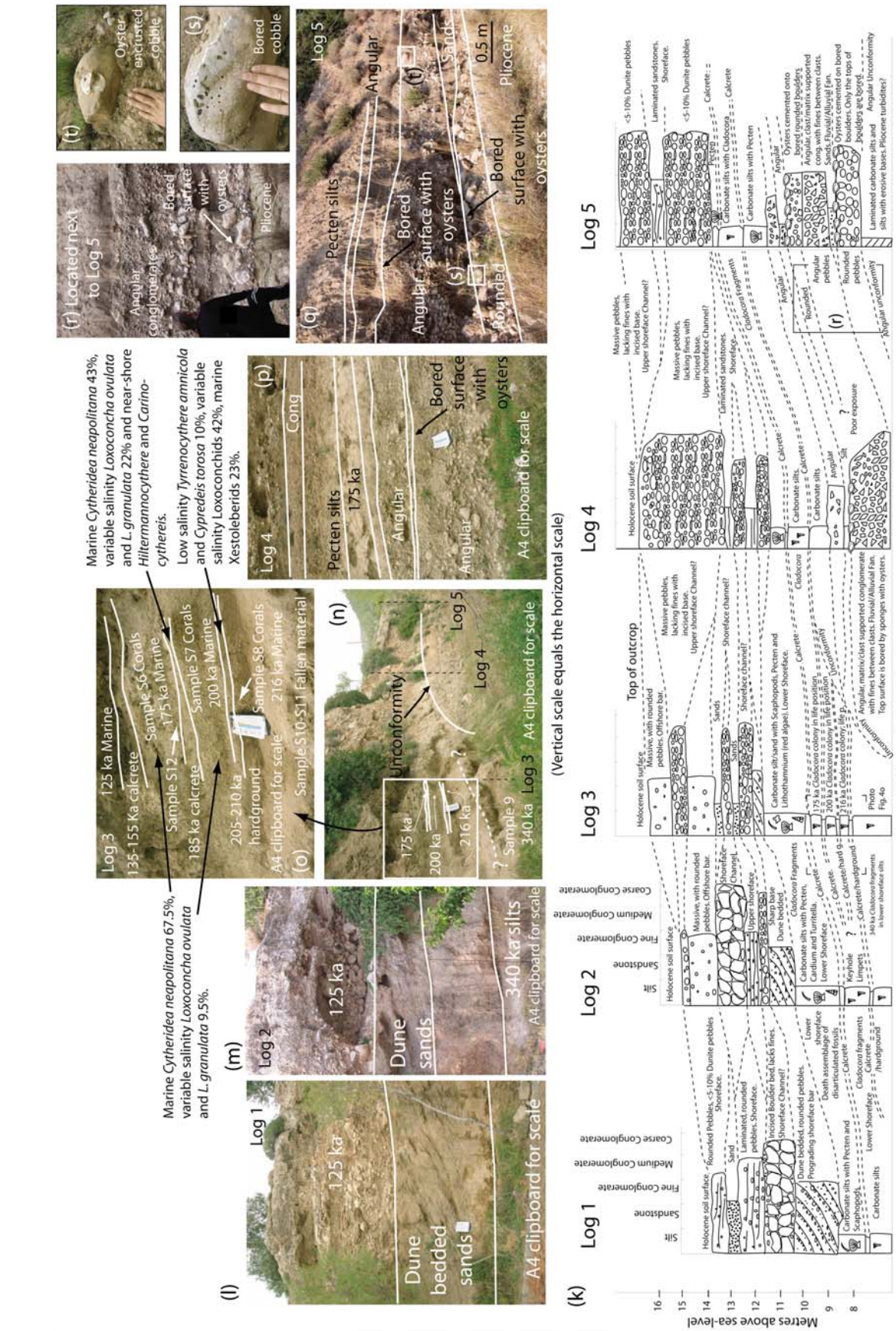

Figure 4. (continued)

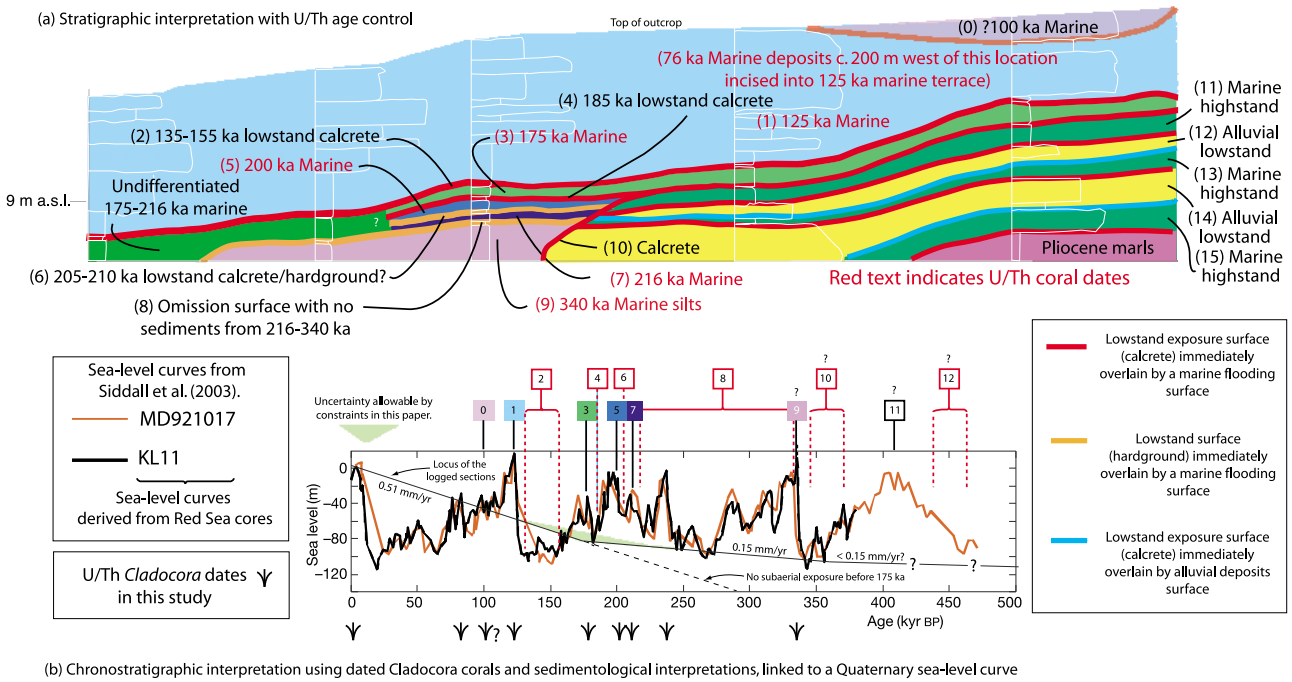

Figure 5. Chronostratigraphic interpretation of logged sections in Figure 4k, supported by ^{234}U-^{230}Th coral dates. Coral dates show that marine sediments were deposited at glacioeustatic sea level highstands (76, 125, possibly 100, 175, 200, 216, 240, and possibly 340 ka), and we correlate these with the global glacioeustatic sea level curve. Lowstand deposits such as subaerial calcretes, subaerial alluvial fan deposits, or marine lowstand hardgrounds occur between the marine highstand deposits. Dates for these lowstand deposits are derived from the sea level curve. The marine to subaerial transitions form when the location emerges above sea level due to uplift and/or falling global sea level. We use the uplift rate scenario implied by dated paleoshorelines on topographic profile 1 (0.15 mm/yr until 175 ka followed by 0.51 mm/yr from 175 ka to present), which runs through the logged sections (Figure 6), to plot the locus of these logged sections on the sea level curve. Our chronostratigraphic interpretation is consistent with the uplift rates in that the sediments in the logged section emerged above sea level at times that agree with the times for the locus in Figure 5b. The uplift rate scenario is consistent with four independent databases: (1) the mapped paleoshorelines on topographic profile 1; (2) the ^{234}U-^{230}Th coral dates; (3) the sedimentology and paleoecology of the logged sections; and (4) the global sea level curve.

section 3.6). The wave-cut platforms are cut into Mesozoic limestones and volcanics or Quaternary cemented alluvial and marine conglomerates. The surfaces themselves are characterized by marine *Entobia* and *Gastrochaenolites* borings, produced by clionid sponges and the bivalve *Lithophaga,* respectively, with shells of the latter present, in places, within the borings. The eroded surfaces typically exhibit decimeter-scale circular depressions where cobbles have scoured down into the surface due to agitation by wave action. Most examples of these wave-cut platforms have a partial veneer of marine sediment with patches of conglomerate a few meters or less in lateral extent. In most cases, the wave-cut platforms are difficult to recognize from aerial photos because of their small size and cover by modern vegetation. However, they are clear both in the field (e.g., Figure 4h), and in places on 1:5000 topographic maps (Figure 3), where they appear as gently sloping benches leading inland and updip to breaks of slope that mark paleoshorelines.

3.3. Shoreface Sediments

[14] In places, shallow marine, shoreface sediments form layered deposits that can be mapped both into wave-cut platforms along strike, and updip into prominent breaks of slope at paleosea cliffs (Figures 3, 4d–4f, and 4k–4t); the shoreface sediments are the lateral age equivalents of the wave cut platforms and paleosea cliffs. The shoreface sediments include upper shoreface cobble-grade conglomerates, pebble-grade conglomerates, medium to course-grained sands, and lower shoreface silts (see Figure 4k for logged sections). The pebbles and cobbles are rounded and composed predominantly of limestones, with some chert and volcanic pebbles. The limestone cobbles and pebbles are bored extensively by marine organisms. The sands and silts contain bivalves, gastropods, coral fragments and in situ coral colonies (*Cladocora caespitosa)* (Figure 4j), echinoids, and the calcareous red algae *Lithophyllum* and *Lithothamnion*. The finer sediments are bioturbated to an extent that primary bed forms indicating currents are rare. Fossil assemblages indicate relative energy levels and paleowater depths, with thin-shelled, articulated bivalve assemblages indicating preservation in low-energy, subwave base environments, and thick-shelled, disarticulated bivalve assemblages indicating preservation in higher-energy, shallower environments (Figure 4k). Thin-shelled bivalve assemblages are associated with in situ, life

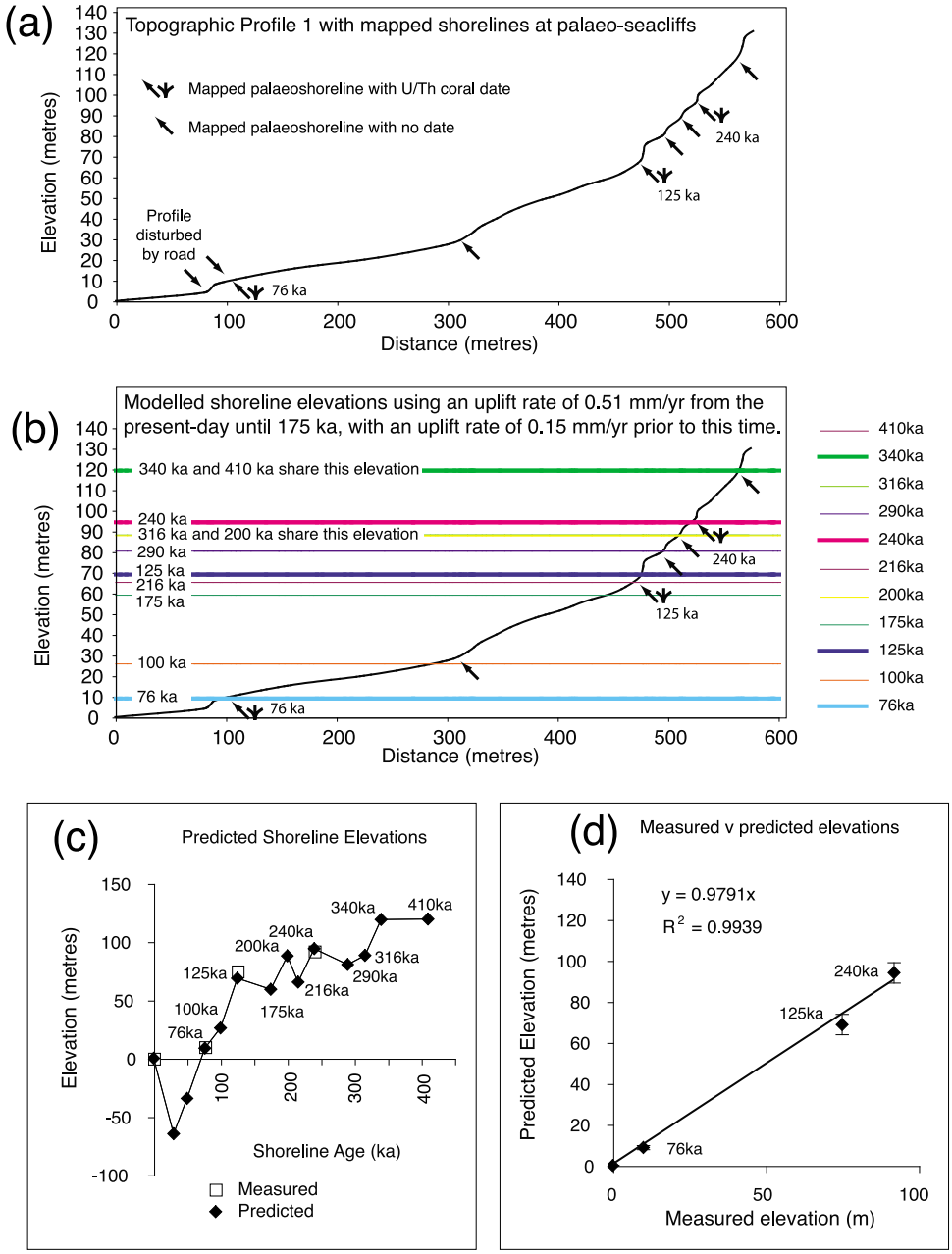

Figure 6. Mapped and modeled paleoshorelines along topographic profile 1 (located in Figure 2b). Paleoshorelines were identified on topographic profile 1 using the features described in the text (wave-cut platforms and shoreface sediments that can be mapped updip in to paleosea cliffs, lithophagid-bored coastal notches or marine subaerial facies transitions). Uplift rates were calculated to explain the elevations of mapped and dated paleoshorelines using initial sea level elevations from the global sea level curve (0.15 mm/yr until 175 ka followed by 0.51 mm/yr from 175 ka to present; $R^2 = 0.99$). These rates were used to calculate the expected elevations of other well-known sea level highstands. These modeled paleoshoreline elevations agree well with the mapped but undated paleoshorelines. We interpret this to mean that the modeled ages are the ages of these undated paleoshorelines. Paleoshorelines from 76, 100, 125, 200, 240, and 340 ka are expected to be preserved, and we have identified them. Paleoshorelines from 175, 216, 290, 316, and 410 ka will be drowned by subsequent sea level rises and subjected to marine erosion; they may not be preserved. However, with the preferred uplift rate scenario, the expected 175, 216, 316, and 410 ka paleoshorelines occupy similar elevations to the 125, 200, and 340 ka paleoshorelines, and the expected 290 ka paleoshoreline elevation is the same as one of our mapped but undated paleoshorelines. We used these correlations between predicted and mapped but undated paleoshorelines to assign ages to undated shorelines on our maps in Figure 3.

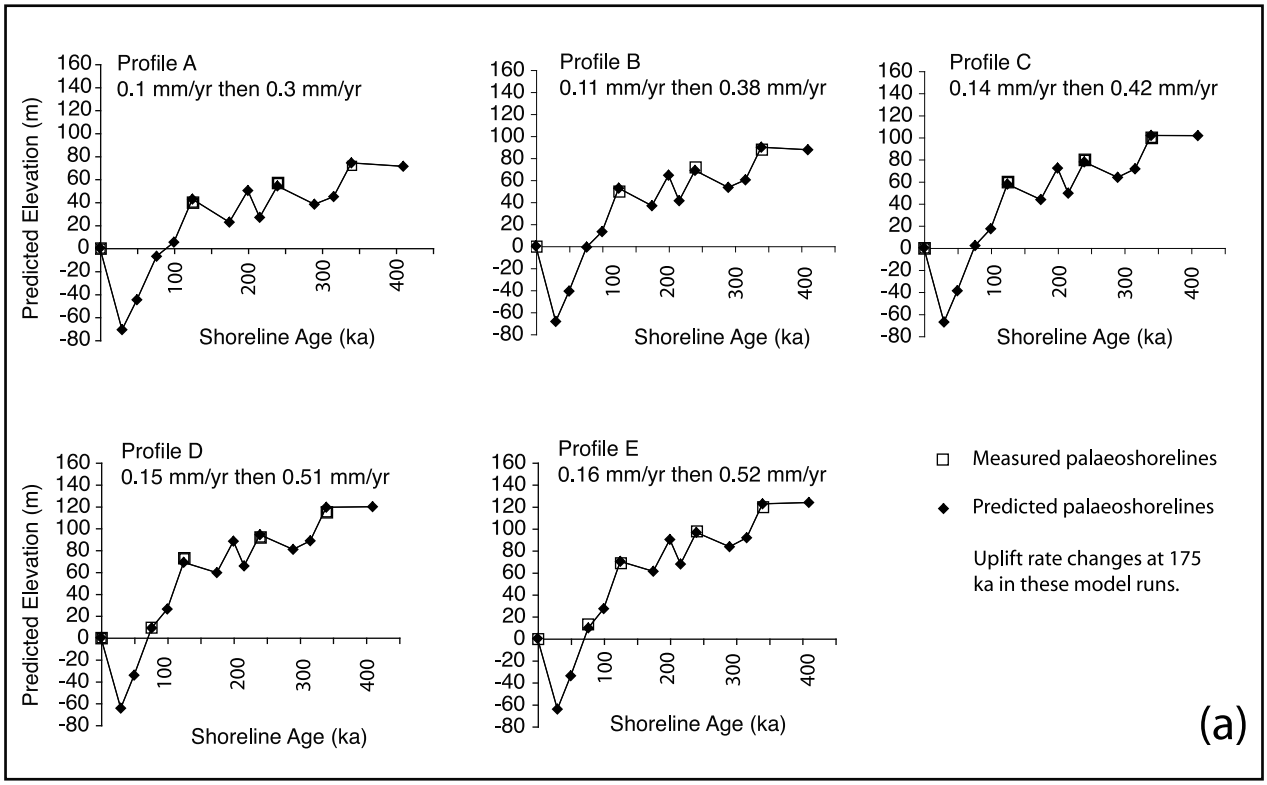

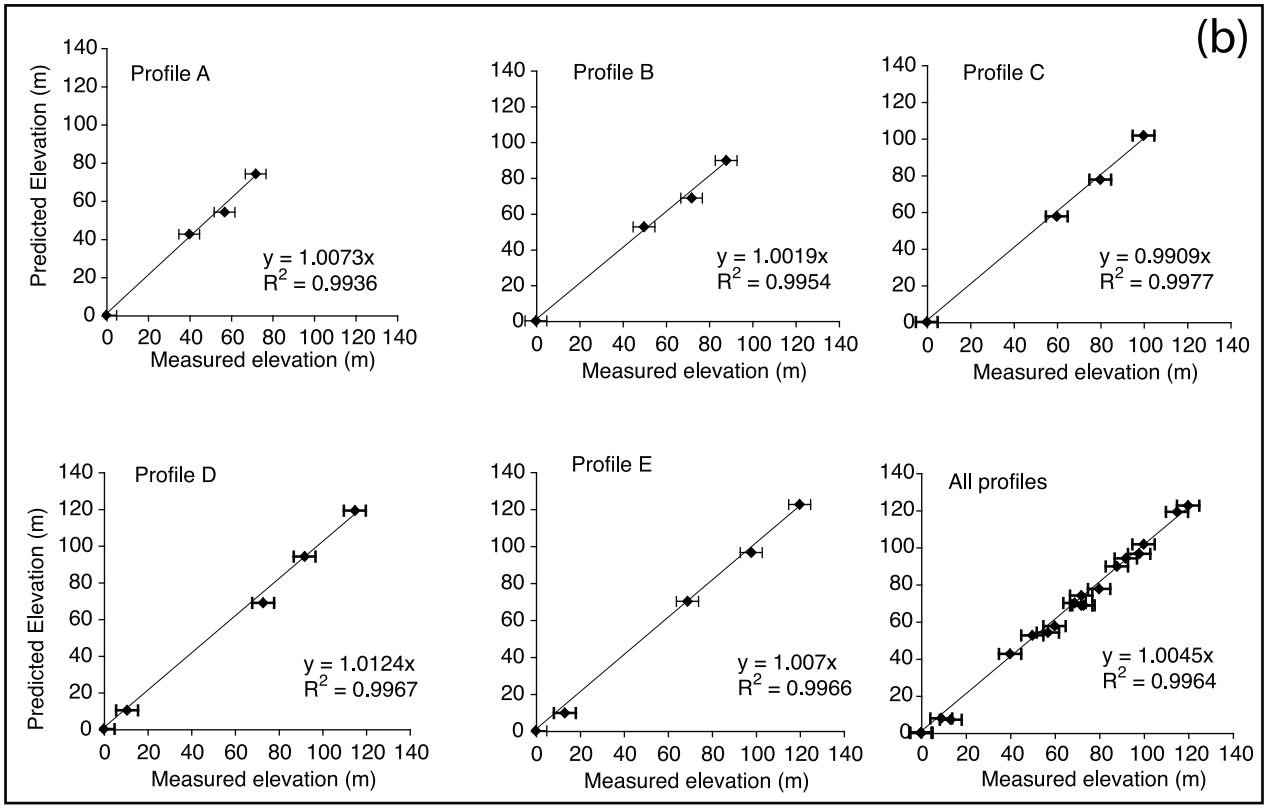

Figure 7. Modeling of the along-strike variation in uplift rate history (see Figure 2f for locations of A–E). Uplift rate scenarios were changed iteratively to explain the mapped and dated paleoshorelines in Figure 3. The change in uplift rate was fixed at 175 ka, guided by the results shown in Figure 6. (a) Comparison of the predicted and mapped elevations of paleoshorelines. (b) Correlations between elevations. Correlations show R^2 values in the range 0.9936–0.9977 for individual locations and an R^2 of 0.9964 for the combined locations. This suggests that we have correctly interpreted the uplift rates (values are shown in Figure 7a and used in Figure 2f).

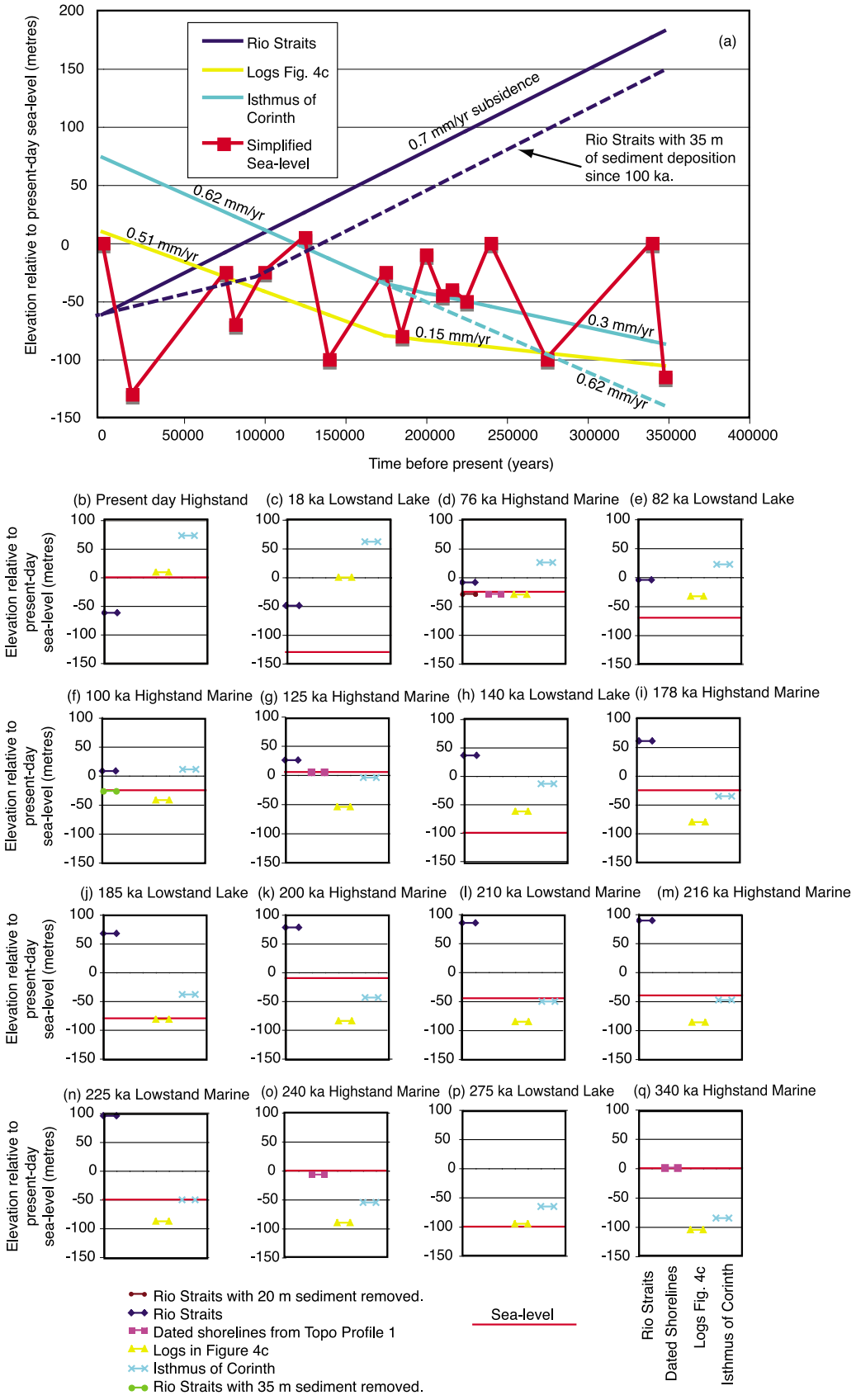
(a)
Rio Straits
Logs Fig. 4c
Isthmus of Corinth
Simplified Sea-level
0.7 mm/yr subsidence
Rio Straits with 35 m of sediment deposition since 100 ka.
0.62 mm/yr
0.51 mm/yr
0.15 mm/yr
0.3 mm/yr
0.62 mm/yr
Elevation relative to present-day sea-level (metres)
Time before present (years)
(b) Present day Highstand
(c) 18 ka Lowstand Lake
(d) 76 ka Highstand Marine
(e) 82 ka Lowstand Lake
(f) 100 ka Highstand Marine
(g) 125 ka Highstand Marine
(h) 140 ka Lowstand Lake
(i) 178 ka Highstand Marine
(j) 185 ka Lowstand Lake
(k) 200 ka Highstand Marine
(l) 210 ka Lowstand Marine
(m) 216 ka Highstand Marine
(n) 225 ka Lowstand Marine
(o) 240 ka Highstand Marine
(p) 275 ka Lowstand Lake
(q) 340 ka Highstand Marine
Rio Straits with 20 m sediment removed.
Rio Straits
Dated shorelines from Topo Profile 1
Logs in Figure 4c
Isthmus of Corinth
Rio Straits with 35 m sediment removed.
Sea-level
Rio Straits
Dated Shorelines
Logs Fig. 4c
Isthmus of Corinth

Figure 8

assemblages of *Cladocora* colonies with preserved upward branching of corallites. The colonies are 0.1–1.0 m in size with the spaces between corallites filled with poorly lithified silts that appear to have been baffled within the coral colonies. At one site, shell beds of *Mytilus* at the base of a mapped paleosea cliff are associated with *Cladocora* fragments indicating a rocky shoreline assemblage.

[15] Within many of the exposed successions there is evidence of relative sea level changes that we use later in the paper to constrain uplift. In places, cemented layers are present within the fine sediments, forming crusty surfaces a few centimeters thick that are lighter in color than the silts in which they occur (see Figures 4n and 4o). These crusts separate units of different grain size and in places occur between vertically stacked *Cladocora* coral colonies. We interpret the crusts as either calcretes indicating subaerial exposure or marine hardgrounds where a relative fall in sea level has caused ravinement, sediment bypass, and subsequent sediment starvation and decrease in sedimentation rate so that marine cementation forms crusts. For one location we studied the ostracod assemblages in an attempt to confirm that the crusts are lowstand deposits between coral-bearing highstand deposits (Figures 4n and 4o). Sediments containing *Cladocora* coral colonies contain marine ostracods such as *Xestoleberis sp*. and *Cytheridea neapolitana* (67.5%), and variable salinity *Loxoconcha ovulata* and *L. granulata* (9.5%). In contrast, the crusts between *Cladocora* coral colonies contain either (1) fewer marine forms (43%), more loxoconchids (22%) and nearshore *Hiltermannocythere* and *Carinocythereis* or (2) nonmarine *Tyrrenocythere amnicola* and *Cypredeis torosa* (10%), Loxoconchids (42%), and marine Xestoleberids (23%). We interpret these ostracod assemblages to indicate that fully marine conditions associated with *Cladocora* coral colonies were interrupted by greater freshwater influence during sea level lowstands, producing calcretes or marine hardgrounds. In section 5, we use coral dates to correlate these relative sea level changes with the Quaternary sea level curve and constrain uplift relative to sea level.

3.4. Intercalated Marine Shoreface and Nonmarine Sediments

[16] In places, the marine sediments are intercalated with clast and matrix-supported angular conglomerates, forming layers a few meters thick (Figures 4p–4r and 4k, logs 4 and 5), that we interpret as nonmarine sediments. The nonmarine sediments have a prominent brown-stained appearance, especially evident within the fine-grained matrix, which contrasts with the yellow-stained, marine-fossil-bearing marine conglomerates with rounded pebbles that lack a fine-grained matrix. We interpret the brown, angular, clast and matrix-supported conglomerates as alluvial fan sediments with both debris flow (matrix-supported) and sheet flood (clast-supported) facies. This is consistent with the fact that we have only found them in locations that can be traced updip into drainage channels and gorges on the present-day coastline.

[17] In places, the top surfaces of these angular alluvial conglomerates are occupied by cemented surfaces that are 10–20 cm thick, composed of rounded pebbles and cobbles that have been bored by marine organisms (Figures 4q–4s). The borings only occur on the top surfaces of the pebbles/cobbles. In places, articulated oysters are attached to the bored cobbles in life position (see logs 4 and 5 in Figures 4k and 4t). These surfaces formed as sea level rose to flood the former alluvial surfaces. Thus, we interpret the intercalations of marine and subaerial alluvial fan sediments as recording relative sea level changes, with relative sea level falls causing forced regression of the shoreline and progradation of alluvial facies. These alluvial surfaces are then reoccupied by the sea during relative sea level rises, evidenced by bored and oyster-colonized pebbles. Initial immersion in seawater evidenced by the borings is followed by deepening indicated by oyster encrustation.

3.5. Logged Sections of Shoreface and Alluvial Intercalations

[18] To document the relative sea level history implied by marine sediments with intercalated calcretes, hardgrounds and alluvial sediments and hence the uplift history relative to global sea levels, we logged five sections through a particularly well-exposed sedimentary section (Figure 4k). Particular features of interest within the section included (1) three distinct in situ coral colonies separated by crusty surfaces within calcareous silts that allow ^{234}U-^{230}Th dating of the section and (2) intercalations of marine and alluvial sediments that can be used to further constrain the relative sea level history.

[19] Overall, our sedimentological interpretation of the logged sections suggests that the sediments record 8–9 relative sea level lowstands (see the key to surfaces in Figure 5). The lowstands must be explained by a combination of the global sea level history, and the uplift rate history we attempt to derive later in the paper.

3.6. Inner Edges of Marine Deposits and Wave-Cut Platforms (Paleoshorelines)

[20] The breaks of slope that form the updip terminations of the wave-cut platforms and shoreface sediments are predominantly cut into limestones and Quaternary conglomerates, but in places are breaks of slope at the transitions from marine shoreface sediments into alluvial angular, clast and matrix-supported breccias. In places, bored notches a

Figure 8. Modeling the entry of the sea into the Gulf of Corinth via the Rio Straits and Isthmus of Corinth through time. The elevation histories of the Rio Straits, the Isthmus of Corinth, the logged section in Figure 4k, and the mapped and dated paleoshorelines on topographic profile 1 were modeled (see Figures 2 and 6). Elevations are shown for these features for times when highstands and lowstands are known from the global sea level curve. The Gulf of Corinth turns into a lake during some glacioeustatic sea level lowstands [e.g., *Collier et al.*, 2000; *Perissoratis et al.*, 2000]. However, using the uplift/subsidence rates and sedimentation rates for the Rio Straits described in the text, marine waters can enter the gulf at all sea level highstands for which we have mapped paleoshorelines showing that they are not lake shorelines, explaining the occurrence of marine corals for which we have ^{234}U-^{230}Th dates.

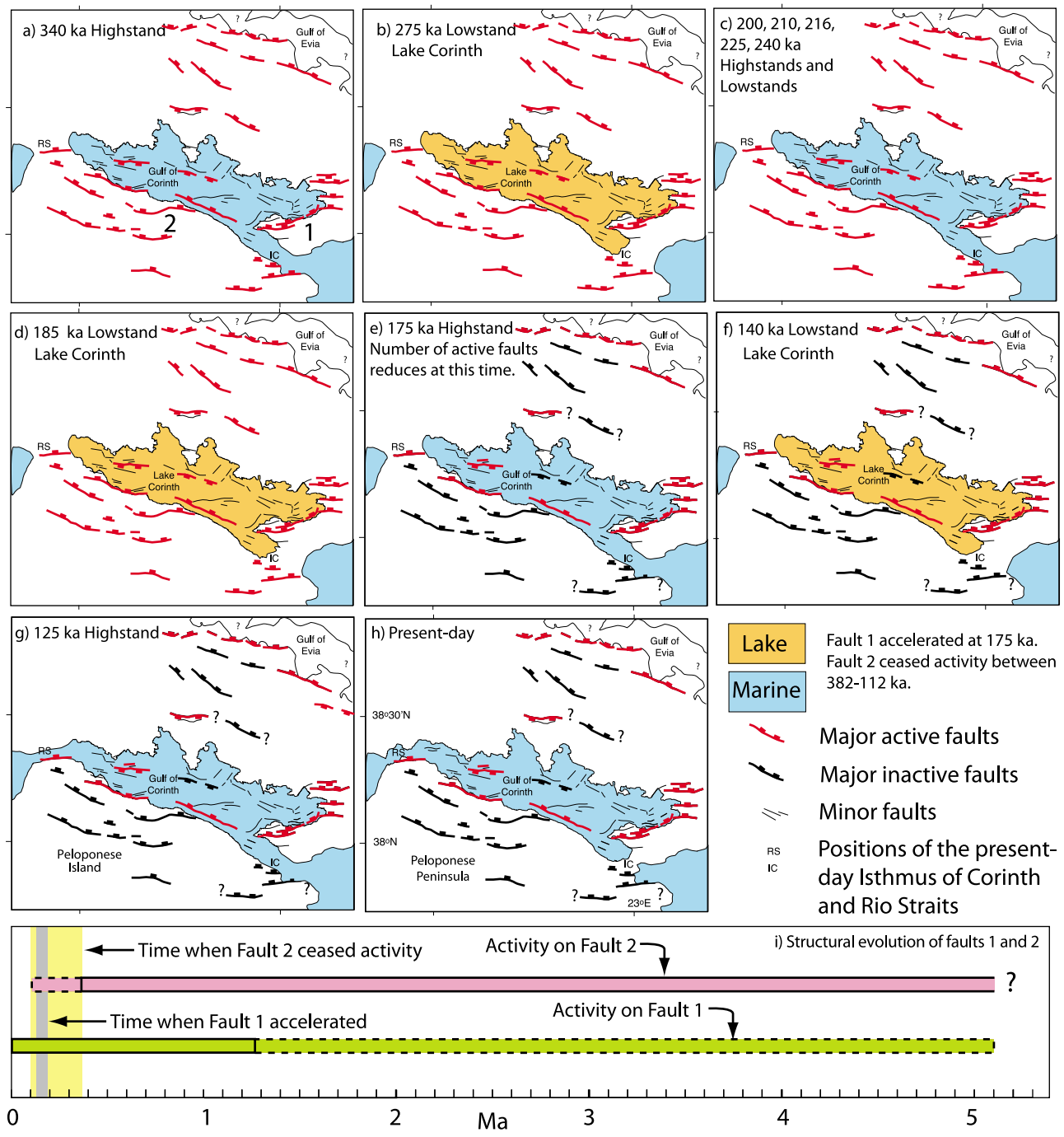

Figure 9. (a–h) Speculative paleogeographic and structural evolution of the Gulf of Corinth and locations of active faults, based on Figure 8. The Gulf of Evia is shown, but no evolution is suggested because of lack of data. Changes in fault length are also not shown because of a lack of data. Shoreline geometries are shown schematically to illustrate opening and closure of the eastern and western ends of the gulf to the Mediterranean Sea. The locations of active faults are speculative, but on the basis of the scenario explained in the text where regional strain rates are maintained as some faults accelerate by cessation of activity on other faults. (i) Activity on faults 1 and 2 shown in Figure 9a, with dashed lines indicating uncertainty in timing. The faults were active synchronously, but fault 1 accelerated when fault 2 ceased activity.

few decimeters in vertical extent indicate marine coastal erosion, analogous to the Holocene notches seen on the modern coast (Figures 4g–4i). These notches occur at the bases of cliffs a few meters to a few tens of meters high (e.g., topographic profile 1, Figure 6a). We interpret these as paleosea cliffs. We interpret both the notches and marine/alluvial transitions as precise indicators of former sea level. Where such indicators can be traced along strike, they

indicate paleoshorelines that would have formed as horizontal features parallel to, and at sea level.

3.7. Mapping Paleoshorelines

[21] To quantify uplift from uplifted paleoshorelines, shoreface sediments and intercalated nonmarine sediments, we mapped at 1:5000 scale, aided by handheld GPS receivers that contained built-in barometric altimeters (vertical precision of a few meters; see Table S1 for details). Topographic maps with elevation contours every 4 m were used as base maps (Figures 3 and S2). We mapped paleoshorelines by identifying wave-cut platforms and associated shoreface sediments, and their landward extent marked by updip breaks of slope. These breaks of slope, as described above, are the paleoshorelines that are located on Figure 3, and given precise coordinates in Table S1. We checked the elevations of paleoshorelines using two barometric altimeters and using the 1:5000 contour maps with contours every 4 m (see Table S1). We are confident that our measured elevations of paleoshorelines are accurate to within $<\pm 2$ m.

[22] At first we concentrated on paleoshorelines that had the most obvious topographic expression and age control from existing ^{234}U-^{230}Th dates. We mapped the 125 ka paleoshorelines to the east away from dated sites reported by *Vita-Finzi* [1993] and *Leeder et al.* [2003] (Figure 2f). We found that this shoreline is tilted, increasing in elevation to the east, as reported by *Morewood and Roberts* [1999] and *Cooper et al.* [2007]. This differs from the interpretation of *Leeder et al.* [2003], who suggest that shoreline is not tilted. However, *Leeder et al.* [2003] only reported paleoshoreline elevations from west of about UTM longitude 667500, studying an area where we record only ~10 m of elevation increase (~40 m increasing eastward to ~50 m); tilting may have been difficult to resolve over this relatively short along-strike distance. We mapped a farther 4 km along strike to the east where the 125 ka shoreline reaches elevations of 70–75 m. Later, we gained a 125 ka ^{234}U-^{230}Th coral date confirming our mapping (sample 2 in Table 1 and Figure 2f). The tilting we report is consistent with the tilted Holocene notches reported by *Cooper et al.* [2007] and the fact that the topography of the peninsula decreases toward the western tip of the fault, which we suggest is due to repeated eastward decreases in coseismic throw in earthquakes like those reported for the 1981 earthquakes (see Figure 2).

[23] To test whether other paleoshorelines are tilted we extended our mapping to include paleoshorelines at higher and lower elevations. In the east of the mapped area we identified seven paleoshorelines, with the number decreasing to three in the western part of the area. The paleoshorelines are tilted with higher tilt angles for higher shorelines (see section 4.2 for ages and tilt angles). This is consistent with progressive deformation and tilting if the higher paleoshorelines are older. However, during the mapping we had no age control. Age control was provided by ^{234}U-^{230}Th dating of *Cladocora* corals.

4. Dating and Initial Constraints on Uplift Rates

4.1. The ^{234}U-^{230}Th Dating

[24] To obtain ages of paleoshorelines and shoreface sediments and hence uplift rates, we collected *Cladocora caespitosa* corals from uplifted marine sediments and obtained ages from 27 samples using the ^{234}U-^{230}Th method (Table 1). We also dated *Cladocora caespitosa* corals found a few meters away from discarded fisherman's nets on the modern beach. These samples were found on the north coast of the Perachora Peninsula, and their pristine appearance suggested to us that these were modern corals that had been living on the present-day seabed. We dated these samples because, if they indeed proved to be modern, they would provide elemental and isotopic data for unaltered samples for comparison with corals from uplifted and presumably older deposits (Table 1).

[25] Each sample of *Cladocora caespitosa* was split into corallite wall and septa samples that were analyzed separately. This was done because septa are very thin, <0.2 mm thickness, while corallite walls are between 0.3 and 0.5 mm in thickness and we suspected the thicker samples might show less alteration and be easier to clean. Sample preparation and analysis followed standard U–series methods [*Edwards et al.*, 1987; *van Calsteren and Schwieters*, 1995].

[26] Prior to TIMS analysis to determine ^{234}U-^{230}Th ages, coral samples were meticulously cleaned. All visual signs of alteration seen under a binocular microscope such as euhedral crystal growths, and rare red/brown coloration, and entrained sediment matrix were removed by scraping with a scalpel. Specimens were then fragmented into millimeter-sized pieces, sequentially washed in 10% hydrochloric acid (Analar) and ultrapure water (UHQ) and dried in a clean environment. The least altered samples were then hand-picked under a microscope. This cleaning and scraping process was repeated until all visual signs of alteration/recrystallization were removed.

[27] Picked subsamples from the above procedure were further assessed for alteration using X-ray diffraction analysis (XRD) and elemental analysis. XRD analyses showed that most samples were dominated by aragonite, with the exception of samples 13, 20, 21, 23, 24 and 26 where a trace of calcite was observed (Table 1). The elemental compositions of samples are typical of modern corals. Concentrations of U for corals from uplifted marine sediments (2.3–3.3 ppm; Table 1) were similar to modern corals and the modern coral we collected (2.342 ppm; Table 1), as are Ca concentrations (38.5–41.8% [*Stirling et al.*, 1995]). Concentrations of Sr (5600–7770 ppm) are similar to those given for corals by *Stein et al.* [1993]. Concentrations of Mg (830–1180 ppm) and Na (3520–3820 ppm) are similar those reported by *Bar-Matthews et al.* [1993]. Samples 25 and 20 were slightly unusual as they showed elevated concentrations of Mg (5015 and 2277 ppm, respectively) and correspondingly high S; this corresponds to the presence of gypsum ~22.5% and halite ~12.5% in XRD results for sample P1/1w; however, no calcite was observed. The presence of gypsum and halite in this sample was attributed to sea spray and resulting mineral deposition.

[28] Values for (^{230}Th/^{232}Th) are greater than 900 for all samples, except the modern coral (sample 27, Table 1) where ^{230}Th/^{232}Th = 168. Typically, a value of <100 for (^{230}Th/^{232}Th), probably indicates the presence of some detrital Th and should be corrected for [*van Calsteren and Thomas*, 2006]; this is not the case for samples in this paper and indicates that both sample integrity and cleaning were excellent.

[29] The (^{234}U/^{238}U) activity ratio of the modern ocean is 1.145 (δ^{234}U(T) = 145). *Stirling et al.* [1995] suggested a

value of δ^{234}U(T) 149 ± 4 was necessary to confirm dates from the 125 ka highstand. Nevertheless, they acknowledge that many samples with δ^{234}U(T) very different from 149 give reliable numerical ages. Samples presented here possess δ^{234}U(T) > 149, as do previous age data reported in the area [e.g., *Dia et al.*, 1997]. However, as we argue below, ages are sufficiently robust to link to the highstands noted by *Siddall et al.* [2003], are consistent stratigraphically within the paleoshoreface sections (Figures 4n and 4o) and mapped paleoshorelines (Figure 3), and are consistent with geomorphic modeling of paleoshorelines for this suite of terraces (see section 5).

[30] The analytical ages derived from the ^{234}U-^{230}Th dating, and the highstand to which we assign each sample are shown in Table 1; details for individual samples are given in Text S1. Errors on the ^{234}U-^{230}Th ages and sample elevations are shown in Figure S1. The uncertainty for different age groupings do not overlap, so we are confident that we have determined ages from distinct time periods and from distinct geomorphic/sedimentary features. In Table 1 (see footnotes b, c, and d), ages identify corals that grew during glacioeustatic sea level highstands at 0, 76, 125, 175, 200, 216, 240, and 340 ka (see Table 1 for explanation of footnotes). Below we use values for which we are confident of the dates and field relationships (footnote b in Table 1) to constrain uplift rates.

4.2. Initial Uplift Rate Determinations

[31] The ^{234}U-^{230}Th dates and paleoshoreline elevations show that paleoshorelines ages increase with elevation. The dates identify the 76, 125, and 240 ka paleoshorelines clearly, and tentatively identify the 340 ka paleoshoreline (Figures 2b, 2f, and 3). Our mapping and dating confirms that tilting is greatest for older paleoshorelines, decreasing for progressively younger ones (gradients are 340 ka, 1.667%; 240 ka, 1.333%; 125 ka, 0.750%; 6386–6500 years B.P., 0.029%; 4356–3700 years B.P., 0.024%; 1691–1900 years B.P., 0.020%; see dates in Table 1 and Figure 2f). The dates also show that the 125 ka paleoshoreline is at ~77% of the elevation of the 240 ka paleoshoreline despite being nearly half its age (Figure 2f). This implies that the uplift rate has increased through time.

[32] The uplift rate since 125 ka is given by our mapping, and our 76 and 125 ka coral dates, the 125 ka dates from *Vita-Finzi* [1993] and *Leeder et al.* [2003] and the study of Holocene coastal notches by *Cooper et al.* [2007]. Our mapping shows that the paleoshoreline dated by the 125 ka coral ages increases in elevation from 40 m in the west to at least 69 m in the east (Figures 2f and 3). Given that global sea level was probably about 5 m above its present-day position at 125 ka [*Siddall et al.*, 2003, *Hearty et al.*, 2007] (Figure 5), this implies a spatial increase in uplift rate for the time period since 125 ka from 0.3 mm/yr in the west to 0.52 mm/yr in the east. Rates as high as 0.52 mm/yr in the east are supported by the existence of the 76 kyr shorelines at 10–15 m (Figures 2f and 3). Sea level at 76 ka was at −30 m relative to the present-day sea level (Figure 5). Thus, 45 m of uplift has occurred in 76 ka, implying an uplift rate of over 0.5 mm/yr (a similar feature may be noted by *Dia et al.* [1997], a 70 ka coral colony reported at 7 m), but the precise location of their coral sample is not given, so it is unclear to us if we have dated the same coral colony). An eastward increasing uplift is also supported by the elevations of Holocene coastal notches [*Cooper et al.*, 2007] (Figure 2e). They suggested that uplift rates have remained constant since 125 ka, increasing from 0.3 to 0.52 mm/yr from west to east, supported by age correlation with radiometric ages on the Holocene notches given by *Pirazzoli et al.* [1994].

[33] Uplift rates prior to 125 ka must have been lower because the 240 ka paleoshoreline occurs at 57 m in the west increasing to 98 m in the east. Although at first sight this implies uplift rates from 0.2 mm/yr in the west to 0.4 mm/yr in the east, the uplift rate was higher than this from 125 ka to the present-day. The precise timing of the uplift rate acceleration is not yet clear; in section 5, we use ^{234}U-^{230}Th dates on the logged sections in Figure 4k to provide extra constraints that show how and when the uplift rate changed.

[34] The ages of the three stacked coral colonies in log 3 (Figure 4k) correlate with known global sea level highstands at 175, 200, and 216 ka (Table 1); ages decrease with elevation because the colonies are in a sedimentary succession. The intervening cemented crusts within marls therefore date from well-known global sea level lowstands at 185 ka and 205–210 ka, consistent with their ostracod assemblages (section 3.3), that indicate increased freshwater influence. The cemented crust within the marl above the 178 ka coral colony is thus younger than 178 ka. It lies beneath more marine sediments that we do not have a date for, but are most likely, following lithostratigraphic correlation with localities along strike (see Figure 3), for which we do have ^{234}U-^{230}Th ages (sample 2 in Table 1), to be from the 125 ka global sea level highstand. Thus, this crust is <178 ka and >125 ka and we suggest it represents the 135–155 ka sea level lowstand. The sediments immediately beneath the 216 ka coral colony are older than 216 ka, and we have a 337 ka *Cladocora* date that we interpret as the 340 ka marine highstand; sediments from the 240 ka highstand appear not to be present in this section. The 340 ka sediments unconformably overlie older sediments (units 10–15 on Figure 5) containing marine/alluvial intercalations, and marls at the base of the section (see Log 6) that are commonly regarded to be Pliocene in age (1.7–5.5 Ma) on lithostratigraphic grounds. We tentatively assign units 10–12 to the Quaternary sea level curve in Figure 5. Quaternary sea level has been no lower in elevation than about −130 m relative to present-day sea level since 0.8 Ma [*Jouzel et al.*, 2007]. Thus, to produce subaerial exposure surfaces (alluvial fan deposits), and marine borings followed by oyster encrustation during rising sea level and transgression in the sediments stratigraphically below the 340 ka corals (units 11–15; see logs 5 and 6), the locality cannot pass permanently beneath the Quaternary sea level on Figure 5. This allows us to perform calculations (section 5) whereby we iteratively change the uplift rate scenario to explain both the elevations of paleoshorelines, and the existence of lowstand subaerial exposure surfaces older than 340 ka.

5. Modeling Uplift

5.1. Uplift Rate for Topographic Profile 1 and the Logged Sections

[35] We conducted iterative calculations to derive an uplift rate scenario that explains (1) the paleoshoreline

elevations and number of paleoshorelines (Figure 2f), (2) the tilting of the paleoshorelines, and (3) the relative sea level history implied by the logged sedimentary sections (Figures 4k and 5). To do this, we utilized knowledge of the upper Quaternary global sea level curve [e.g., *Siddall et al.*, 2003] (Figure 5b). Our aim was to identify the ages and thus to explain the occurrence of all the paleoshorelines shown on Figure 2f, some of which we have been unable to date with ^{234}U-^{230}Th determinations of coral ages. An uplift rate scenario that achieves the above must also explain the existence of eight to nine sea level lowstands in the logged section shown in Figures 4k and 5.

[36] We constructed a topographic profile (topographic profile 1, Figure 6 and located in Figures 2b and 3a), which runs across the area of highest uplift and the largest number of paleoshorelines, and has the logged sections of Figures 4k and 5 at its base. Topographic contours every 4 m allow construction of a relatively precise topographic profile that has clear breaks of slope (paleosea cliffs) that indicate our mapped paleoshorelines. We conducted calculations that (1) predicted the elevations of the 76 and 125 ka paleoshorelines, because it appears that the uplift rate has been constant over this time period [*Cooper et al.*, 2007] and (2) predicted the elevations of the 240 and 340 ka paleoshorelines. Because the uplift rate was lower prior to 125 ka, we iteratively changed (1) the time when the uplift rate changed and (2) the uplift rate prior to this change.

[37] After a number of iterations, the best fit to measured versus predicted paleoshoreline elevations was achieved with an uplift rate of 0.51 mm/yr from the present-day until 175 ka, with an uplift rate of 0.15 mm/yr prior to this time ($R^2 = 0.99$; Figure 6). Error bars for ages of the highstands and mapped paleoshoreline elevations were extrapolated, and they allow a more gradual change in uplift rate from 0.15 to 0.51 mm/yr at 175 ± 75 ka (see Figure 5b). This uplift rate scenario also predicts the elevations of well-known sea level highstands from global sea level curves that we have been unable to date (compare Figures 6a and 6b). We note a very good correlation between the predicted elevations of paleoshorelines and mapped paleoshorelines for which we have not managed to gain radiometric dates (Figure 6b). In particular, we note the predicted elevations of the 100, 290, 316, 200, 340, and 410 ka highstand paleoshorelines pass within a few meters of our mapped paleoshorelines. If we assign these ages to the mapped paleoshorelines we gain a predicted versus measured elevation correlation with $R^2 = 0.9958$ (not shown), although we admit there is an element of circular reasoning for this point. Nevertheless, the predicted elevations fall close to elevations where we have mapped paleoshorelines. We interpret this as supporting our uplift rate scenario. Note that our interpretation predicts that paleoshorelines of different ages will, in places, occupy the same elevations. This is because sea levels for past highstands were at a variety of paleoelevations above and below present-day sea level [*Siddall et al.*, 2003] (see Table S2) (Figure 5b). For example, the 340 and 410 ka paleoshorelines are predicted to both occupy an elevation of 120 m, with those for 316 and 200 ka at 90 m (Figure 6b). The 125, 216, and 175 ka paleoshorelines are predicted to be within 10 m of each other (60–70 m elevation), perhaps explaining why the paleoshoreline(s) at this elevation is/are very obvious in the topographic profile (Figure 6b). The complexity of paleoshoreline elevations resulting from a given uplift rate scenario, but with differing initial sea level elevations, is shown in Figure 6c. The curve shows that paleoshorelines for 175, 216, 290, and 316 ka will be degraded by marine erosion at subsequent highstands (e.g., the 216 ka paleoshoreline will be eroded as the 200 ka sea level transgresses this location; the same is true of the other mentioned paleoshorelines). Thus, we do not expect to find paleoshorelines from 175, 216, 290, and 316 ka. However, it appears that the bedrock is sufficiently resistant to erosion during rising sea level to allow paleoshorelines to be preserved from 290 ka (see Figure 6b); the 175, 216, and 316 ka paleoshoreline locations are coincident with paleoshorelines that we expect to be preserved.

[38] Although the preferred uplift rate scenario predicts the elevations of paleoshorelines dated with coral ages extremely well ($R^2 = 0.99$; Figure 6d), we also need to consider whether this explains the sedimentary succession in the logged sections at the base of the profile (Figures 4k and 5). We have plotted the uplift rate scenario onto the sea level curve (Figure 5b). Note that the curve represents the locus of the logged sections through time relative to sea level. Where the locus is above sea level, we expect to find evidence of subaerial exposure, with marine transgressions when the curve falls below rising sea level. The logged sections contain deposits that coral ages suggest were deposited at sea level lowstands (e.g., the lowstand crusts at 185 ka, unit 4 in Figure 5b, and 205–210 ka, unit 6 in Figure 5b, that occur between the 178 and 200 ka and between 200 and 216 ka coral colonies in log 3; Figure 4k). The locus of the logged sections is beneath the sea level curve for 205–210 ka so this logged horizon is a marine hardground formed during a global sea level lowstand. The locus of the logged sections rises just above the sea level at 185 ka so this logged horizon is a subaerial calcrete formed at a global sea level lowstand. Thus, our preferred uplift rate scenario explains both the sedimentology of the section and the Ostracod assemblages we have documented. Note also that uplift rates higher than 0.15 mm/yr for the period before 175 ka could not explain the subaerial exposure (alluvial fan sediments) we have observed in the logged sections beneath the 340 ka marine silts (unit 9); if unit 12 is really from circa 450 ka, and the sea level shown by *Siddall et al.* [2003] is correct, uplift rates would have to be even lower than 0.15 mm/yr; this needs further work.

[39] In summary, the uplift rate scenario, where uplift proceeded at 0.15 mm/yr until 175 ± 75 ka and then accelerated to 0.51 mm/yr explains both the mapped and dated paleoshoreline elevations, and dated sedimentary sections along the line of topographic profile 1.

5.2. Variation in the Uplift History Along Strike

[40] Further modeling was conducted to explore uplift rate scenarios that would explain the uplifted paleoshorelines to the west of topographic profile 1, further along strike (Figures 2f and 7). We modeled the elevations of paleoshorelines on profiles A–E located on Figure 2f. We used the same paleosea level elevations for Figure 6 (see Table S2) and again used 175 ka as the time when the uplift rate accelerated. We iteratively changed the uplift rates before and after this change in an attempt to replicate the measured paleoshoreline elevations.

[41] The results (Figure 7) show excellent correlations between measured and predicted shoreline elevations ($R^2 =$

0.996). The implied uplift rates vary from 0.1 to 0.16 mm/yr from west to east for the time period before 175 ka and from 0.3 to 0.52 mm/yr from west to east for the time period since 175 ka.

[42] The decrease in uplift rates from east to west is consistent with our interpretation that uplift during the upper Quaternary and Holocene is due to repeated coseismic rupture of the fault that hosted the 1981 earthquake, with uplift rates decreasing toward the western tip of this fault. This is consistent with the westward decrease in footwall topography and coseismic throws for the 1981 earthquake. Our interpretation differs from that of *Leeder et al.* [2003, p. 1, 2005, p. 555], who suggest that this part of the Perachora Peninsula is part of a "uniformly-uplifting crustal terrane" with "little evidence for regionally-significant late-Quaternary faulting," and with the "elevation of both Holocene and Late Quaternary shoreline features showing no systematic changes" [see also *Turner et al.*, 2008]. Our interpretation also differs in that they suggest the existence of uplifted deposits from isotope stage 5a (76 ka) onshore just to the west of Agroliou Bay (Figure 2b), whereas our preferred uplift rate scenario implies that 76 ka marine deposits would still be below present-day sea level in this location (see Figure 2f). The high uplift rates in the east in our interpretation are consistent with at least some of the coral dates of *Dia et al.* [1997] if the location of their 70 ka coral date from 7 m elevation is the same as that where we report 76 ka from ~10 m (see section 4.2).

[43] Further support for fault displacement gradient-controlled uplift is that paleoshorelines show flat portions within their profiles between UTM longitudes 667000 and 668500 (see gray boxes on Figures 2e and 2f). These are areas where the fault strike changes, bringing the fault and hence the cause of the uplift closer to the paleoshorelines, allowing relatively high uplift rates to persist farther to the west than they would if the fault had maintained its strike (that is, flat portions on the uplift profiles). Thus, the uplift is sensitive to proximity to the fault (when the fault is 500 m closer to the paleoshorelines the uplift is increased by about 0.1 mm/yr), supporting our interpretation that uplift is fault controlled. This sensitivity is inconsistent with the idea that uplift is dominated by other faults located offshore to the north and south of the peninsula such as the Loutraki fault and the Strava fault (Figure 1) and confirms that uplift of the paleoshorelines we have mapped is dominated by slip on the fault that ruptured in the 1981 earthquakes.

[44] Overall, our study suggests that uplift in the footwall of the fault that experienced the 1981 earthquakes varied spatially both before 175 ka and since 175 ka, with rates decreasing toward the western fault tip due to displacement gradients that developed during repeated coseismic displacement during the upper Quaternary and Holocene. The uplift rates increased by a factor of 3.4 at the location of topographic profile 1. The average for profiles A–E is an uplift rate acceleration by a factor of 3.2 ± 0.2, where 0.2 is one standard deviation.

6. Sea Level in the Gulf of Corinth and Rio Straits and Isthmus of Corinth

[45] We have so far assumed that a marine sea level curve should be used for the above modeling, but it is well known that the Gulf of Corinth turns into a lake at global sea level lowstands, due to a shallow bathymetric sill at −60 m at the Rio Straits in the western Gulf [e.g., *Perissoratis et al.*, 2000; *Bell et al.*, 2008]. Could it be that some of the paleoshorelines are actually former shorelines of Lake Corinth and thus may not correlate with global sea levels? Here we explain why we think all the paleoshorelines we have measured are marine, and why we are correct that a marine sea level curve should be used in our uplift calculations (see Figures 8 and 9).

[46] First, paleoshorelines dated with coral dates are clearly marine. We have corals dated to 76 ka, (possibly) 100, 125, 178, 200, 216, 240, and 340 ka (Table 1). Clearly, the Gulf of Corinth was marine at these times, and a global sea level curve applies.

[47] Second, we have reconstructed the paleogeography of the Gulf of Corinth. This is based on our assessments of the rates of vertical motion at the Rio Straits and the Isthmus of Corinth. We used these values to see if the sea could enter the area where we report paleoshorelines at the times we suggest. Our interpretation differs from that of previous studies [e.g., *Westaway*, 2002; *Bell et al.*, 2008], mainly because we investigate the possibility that the elevation of the Rio Straits (presently 60 m below sea level), which forms the western inlet of the Mediterranean Sea into the Gulf of Corinth, may change through time due to active faulting.

[48] The Rio Strait is located in the hanging wall of an active normal fault, close to measured extension rates of 15–20 mm/yr [*Briole et al.*, 2000]. With such high rates of extension, we think it is unlikely that the Rio Strait is stationary in elevation, and is most likely subsiding in the hanging wall of the fault (Figure 1). We know of no data constraining the rate of subsidence. *Houghton et al.* [2003] report an uplift rate in the footwall of this fault of 0.7–0.8 mm/yr, based on ^{234}U-^{230}Th coral dates of 175 ka at 110 m near a prominent paleosea cliff. Uplift/subsidence ratios on normal faults decrease from around 1:6 during coseismic deformation [*Stein and Barrientos*, 1985] to about 1:2 after postseismic relaxation [*McNeill and Collier*, 2004]. If we are conservative and suggest that subsidence matches the rate of footwall uplift (i.e., 1:1), the Rio Straits are subsiding at 0.7–0.8 mm/yr. This implies that the Rio Straits would be above sea level prior to 12–15 ka (Figure 8). The Rio Straits would not be an access point for the sea to enter the area of the Gulf of Corinth at any point in time before this. Using a higher subsidence rate (e.g., an uplift/subsidence ratio of 1:2) makes the situation worse. The question then arises as to how seawater entered the Gulf of Corinth before this time, evidenced by marine fossil corals that we have dated. The answer must lie in the fact that the Isthmus of Corinth is uplifting [*Mariolakos and Stiros*, 1987]. *Collier et al.* [1992] showed that fossil corals can be found on top of the Isthmus of Corinth along the famous Corinth Canal section, and farther inland, and shallow marine conditions (~10–15 m water depths) are confirmed by the existence of subaqueous dunes of oolitic limestone [*Collier and Thompson*, 1991]. The warped surface of the isthmus [*Mariolakos and Stiros*, 1987], shows that uplift rates increase from the south to the north, from 0.16 mm/yr [*Collier et al.*, 1992] to as high as 0.4–0.8 mm/yr (supported by the existence of marine deposits from the "last two circa 100 ka glacioeustatic cycles" at ~150–155 m [*Collier and Dart*, 1991] (205 ka

[*Collier et al.*, 1992]) [see also *Roberts*, 1996b; cf. *Westaway*, 2002]. It appears that seawater was able to enter the Gulf of Corinth over the Isthmus of Corinth, which had not yet uplifted enough to emerge above sea level and become an isthmus. The question is at what times did seawater enter the Gulf of Corinth through this inlet? We extracted the topography of the present-day isthmus from a SRTM 100m DEM and the published 1:50000 topographic map. The lowest traverse that can cross the isthmus has a maximum elevation of ~73 m. Through comparison with the sea level curve, an uplift rate of 0.62 mm/yr at the Isthmus of Corinth implies that seawater could access the Gulf of Corinth at all the highstands we claim are marine, except the 76 ka marine highstand and the 100 ka marine highstand (Figure 8). This is true if we use a constant uplift rate of 0.62 mm/yr or if we reduce the uplift by a factor of 3.2 prior to 175 ka, assuming that uplift of the Isthmus of Corinth is controlled by the fault that ruptured in the 1981 earthquakes. For the Isthmus of Corinth, we show uplift rates of 0.62 mm/yr since 175 ka and 0.3 mm/yr before then as an example in Figure 8. Returning to the 76 ka highstand, we have dated corals at 76 ka so we know this is a marine incursion into the Gulf of Corinth, despite our modeling implying that both the Rio Straits and the Isthmus of Corinth were above sea level, turning the gulf into a lake. However, if, for example, >15 m of sediment have accumulated at the Rio Straits since 76 ka, a value that is not unreasonable given the 40 m of sediment that has accumulated at some places in the Rio Strait in the Holocene, and the existence of at least 40 m of sediment beneath the present-day seabed [*Perissoratis et al.*, 2000], seawater could have entered the Gulf of Corinth at 76 ka through the Rio Straits (we show 20 m sediment removed at the Rio Strait for 76 ka; Figure 8a). We also show 35 m of sediment removed since 100 ka to illustrate how much sediment would be needed to make this a marine incursion through the Rio Straits, and note that we have a 115 ka *Cladocora* date from Heraion (sample 25 in Table 1), that although we note had gypsum and halite in the sample prior to cleaning, could confirm a 100 ka marine incursion. We also have a mapped paleoshoreline at the elevation where the 100 ka paleoshoreline is expected following our modeling (Figure 6b). Overall, we suggest that the sea could enter the Gulf of Corinth through the Rio Straits at 0, 76, 100, and 125 ka; the sea could enter the Gulf of Corinth through the area that would become the Isthmus of Corinth at 125, 175, 200, 216, 240, and 340 ka (Figures 8 and 9). Note that both the western and eastern ends of the Gulf of Corinth were open to the sea at 125 ka. Thus, all the paleoshorelines that we have claimed are marine can be explained with reasonable uplift/subsidence rates at the Isthmus of Corinth and the Rio Straits, and most are supported by *Cladocora* dates, justifying our use of the global Quaternary sea level curve for our modeling.

7. Discussion

[49] Our results suggest that at 175 ± 75 ka, the uplift rate on the south coast of the Perachora Peninsula increased by a factor or 3.2 ± 0.2, with a spatial variation in uplift that is controlled by the lateral decrease in cumulative upper Quaternary/Holocene slip toward the tip of the fault that ruptured in the 1981 Gulf of Corinth earthquakes. As the ratio between uplift rate and slip rate is most likely constant over periods of time containing many seismic cycles, we infer that the slip rate on the fault increased at 175 ± 75 ka by a factor of 3.2 ± 0.2. This increase in slip rate is consistent with the findings of *Sakellariou et al.* [2007], who studied seismic reflection profiles across the synrift sediments that have accumulated in the hanging wall of the same fault. They suggest that at about 130 ka, slip rates increased, as they claim that there was an increase in sedimentation rate at that time. We note that *Sakellariou et al.* [2007] have no age control on the horizons at depth so we cannot be sure about the timing or existence of the slip rate acceleration from their data alone. However, we note the similarity in timing of their interpreted increase in slip rate and the slip rate increase that we have measured with ^{234}U-^{230}Th coral date age control. The timing of the 175 ± 75 ka slip rate increase also coincides with cessation of slip on a neighboring fault. *Flotté et al.* [2001] provide ^{234}U-^{230}Th dates for carbonate cements within fault rocks that show a neighboring fault was active at 382 ka, evidenced by deformed carbonate cements of this age but became inactive by 112 ka, evidenced by undeformed carbonate cements that cover and seal the fault rocks. It appears that acceleration of slip on one fault coincides with cessation of slip on a neighboring fault.

[50] An acceleration in slip rate is important for three reasons. First, it means that one cannot simply assume constant rates of vertical motion when attempting to assess the ages of uplifted or downdropped paleoshorelines where poor age constraints exist. Second, it impacts on the age relationships between the active and inactive faults around the Gulf of Corinth because the slip rate is commonly used to back strip the total slip to derive the time when a fault began to slip. Third, the extra strain per unit time implied by acceleration of the slip rate must be explained in terms of its relationship with regional strain rates and mechanisms of extension. We discuss each of these in turn below.

7.1. Age Constraints on Paleoshorelines

[51] The classic marine terrace sequence that has been uplifted and deformed on the southern coast of the Gulf of Corinth (Figure 1) has relatively poor age constraints. Previous studies have tried to assess the ages of the paleoshorelines associated with the terraces in order to constrain the rates and timescales for the deformation and hence the mechanisms responsible [e.g., *Armijo et al.*, 1996; *Westaway*, 1996, 1998, 2002, 2007]. However, ^{234}U-^{230}Th coral dates are restricted to the lowest terraces, with the ages of higher terraces either assumed using constant uplift rate calculations or constrained using questionable nannoplankton biostratigraphy (see *Westaway* [2002] for a discussion). Although we present no new data for these terraces herein, we point out that the possibility of a slip rate increase at 175 ± 75 ka has not been explored in detail for the Xylokastron Fault which has been suggested to be responsible for the uplift of the terraces; this should be reexamined. This is also true of downdropped paleoshorelines and marine strata. Although the interpretation of *Sakellariou et al.* [2007] is consistent with our interpretations, we note that they have no age control on horizons at depth. The same is true of *Bell et al.* [2008, p. 158], who interpret the ages of end lowstand shorelines from depth converted seismic reflection data in the hanging wall of the North Eratini Fault (Figure 1), although there are "no core

data in this area to verify our age assignments." Clearly, a key to deciphering the subsidence history for the Gulf of Corinth would be to gain dated cores to calibrate seismic reflection data for synrift sediments, and constrain the chronology of faulting. Until such data are gathered we suggest that it will be difficult to confirm or refute the hypothesis that seismic reflection data are consistent with the slip rate increase we have measured at 175 ± 75 ka (see section 7.2).

7.2. Age Relationship Between Active and Inactive Faults

[52] We can use the proposed slip rate acceleration to calculate whether activity on presently active and presently inactive faults overlapped in time or occurred sequentially (section 1). *Collier et al.* [1998] provide a rate of vertical offset from a paleoseismic trench study of offset Holocene deposits across the 1981 surface ruptures, close to the center of the fault (T in Figure 1). They report rates of vertical offset for normal faulting of 0.7–2.5 mm/yr. The total vertical offset due to normal faulting at this trench site is known from the offset of the base of an ophiolitic thrust sheet (dating from the Cretaceous-Tertiary Alpine compression), exposed both in the hanging wall and the footwall of the presently active normal fault. The total vertical offset is about 1.2 km [*Roberts*, 1996b]. Using rates of vertical offset of 0.7–2.5 mm/yr back to 175 ka and these same rates reduced by a factor of 3.2 prior to 175 ka, it would have taken 5.1–1.2 Myr to accumulate 1.2 km of vertical offset. This implies that the faulting began at 5.1–1.2 Ma (Figure 9). These ages overlap with those for faulting on Plio-Pleistocene normal faults to the south and north of the Gulf of Corinth. Indeed, ^{234}U-^{230}Th dating of carbonate cements within fault rocks shows that one of them was active as recently as 382–112 ka [*Flotté et al.*, 2001].

[53] The important implication is that for faults that were active synchronously prior to >112–382 ka, the slip rate on one fault accelerated while that on another ceased or decreased, and these events both occurred within the time period that brackets the age of cessation of fault activity on the second fault (175 ± 75 ka slip rate acceleration and 382–112 ka cessation of slip) (Figure 9). We do not know whether this applies to all the active and inactive faults on Figure 1, due to a lack of data. However, *Bell et al.* [2008] provide observations that may support this interpretation of a major change in fault related vertical movements at circa 175 ka. They provide seismic reflection data with exquisite detail that reveal the presence of four lowstand shorelines in the hanging wall of the North Eratini Fault (Figure 1), each of which is covered by a marine flooding surface. Beneath this, the data reveal a major unconformity (U on Bell et al.'s Figure 3), overlying a unit with less clear reflections. They interpret the ages of the flooding surfaces as the 340, 240, 130, and 12 ka sea level rises because of a stationary Rio Straits assumption, with the age of unconformity U estimated to be circa 0.4 Ma. However, as they have no age control from a borehole, an alternative interpretation is permitted by the data. If the flooding surfaces relate instead to sea level rises culminating at 125, 100, 76, and 6 ka, the ages of sea level rises confirmed by our ^{234}U-^{230}Th coral dates, the unconformity U would then be circa 175 ka in age, the time when we suggest a reorganization of slip rates occurred in the Gulf of Corinth. The implications of the similarity in timing between (1) the slip rate acceleration we have measured at 175 ± 75 ka (this study), (2) the 382–112 ka cessation of slip on a neighboring fault [*Flotté et al.*, 2001], and (3) a possible unconformity at circa 175 ka near the North Eratini Fault [*Bell et al.*, 2008] are intriguing, and we discuss this below.

7.3. Strain Localization Through Time

[54] The extra strain per unit time implied by acceleration of the slip rate must be explained in terms of its relationship with regional strain rates and mechanisms of extension. It could be that (1) the rate of far-field extension increased at 175 ± 75 ka or (2) strain was redistributed at this time when slip on faults to the south of the gulf ceased or decreased. We are aware of no evidence that supports the idea that the rate of far-field extension increased at 175 ± 75 ka. In any case, it is difficult to envisage how such an increase could explain why some faults ceased or decreased in activity at this time [*Flotté et al.*, 2001]. However, the second possibility could be consistent with the ideas of *Gupta et al.* [1998], *Cowie and Roberts* [2001], and *Cowie et al.* [2005], who suggest that regional strain rates are maintained during the geometrical evolution of a fault system, so that the growth in size of some faults causes other faults in the system to cease activity. Specifically, following *Cowie and Roberts* [2001], the strain represented by a fault of length, L, and downdip width, W, depends on the geometric moment, $M_g = dA$, where fault plane area $A = LW$, and W depends on the thickness of the faulted layer [*Kostrov*, 1974]. According to the displacement-length scaling relationship $d_1 = \gamma L_1$, faults of length L_1 represent a strain $M_g = \gamma L_1^2 W$, whereas a larger structure that is developing through growth of the original smaller structures with a fully readjusted (self-similar) profile will eventually represent a strain $M_g = \gamma L_2^2 W$ (using $d_2 = \gamma L_2$). Note that $L_2 = NL_1$. It follows that the strain accommodated by the larger structure (with $d_2 = \gamma L_2$) is N times larger than that for the early faults, assuming W remains constant. In order for the regional strain rate to remain constant the spacing between those faults that remain active must change. In other words, some faults located across strike from faults that accelerate must cease or decrease in activity. We suggest that growth of faults in the Gulf of Corinth region may have produced an acceleration of the slip rate on some faults in an attempt to achieve a future value of d_2; this redistributed regional strain rates causing some faults to cease or decrease their activity. In this scenario, early deformation may have occurred across the entire region with all the faults shown in Figure 1 active (see Figure 9 for a speculative reconstruction of the geography of fault activity). This was followed by growth and interaction between the faults, so that some faults, specifically those to the south of the Gulf of Corinth and those between the Gulf of Corinth and the Gulf of Evia, ceased or decreased in activity. If this is true, the velocity field measured with GPS shown in Figure 1 only applies back to 175 ± 75 ka; the strain was more distributed prior to this time. This is a testable hypothesis given that most of the onshore faults in Figure 1 have either associated paleoshorelines or well-exposed synrift sequences that are amenable to further study to derive fault-specific displacement histories, and offshore faults are constrained in terms of the geometry of their synrift sediments, but await age control from a well [see *Bell et al.*, 2008].

[55] It would not be surprising if initial distributed faulting has been followed by localization of strain onto faults within the zone of formerly active faults, as this is precisely the style of fault activity documented for the northern North Sea, the Gulf of Suez and the Gulf of California [*Cowie et al.*, 2005, 2007]. However, what is surprising is how rapidly this transition appears to have occurred in the Gulf of Corinth. Our data suggest that the factor of 3.2 ± 0.2 slip rate increase on the fault we studied occurred in 0.15 Ma (175 ± 75 ka) and that this may be a sign that slip became localized in the present-day Gulf of Corinth over this time interval. For comparison, in the North Sea, extension across the Hutton, Murchison, Brent-Statfjord, Gullfaks, Snorre, and Visund normal faults initiated at 167–155 Ma, but localized onto the Gullfaks and Visund faults from 155 to 140 Ma increasing their slip rates by a factor of ~8 (~0.06 to ~0.5 mm/yr); localization occurred over several million years [*Cowie et al.*, 2005]. Thus, if the slip rate acceleration we have measured on one fault implies regional strain reorganization, the process of strain localization in the Gulf of Corinth appears to have been an order of magnitude faster than in the North Sea, concomitant with the higher slip rates in the former [*Cowie et al.*, 2005].

[56] We argue that the rapidity of the slip rate changes places constraints on the possible processes responsible for the reorganization of the geography of active faulting and localization if this is what has occurred. The slip rate reorganization occurred rapidly at 175 ± 75 ka (0.15 Ma), so the mechanism responsible must have a response time of $\sim 10^5$ years. It seems unlikely that large-scale effects such as buoyancy forces, thermally induced changes in mantle viscosity, or variations in the geometry and location of a subducted slab could change significantly on a 10^5 year timescale. With rates of rotation about vertical axes measured by paleomagnetism and inferred from geodetic measurements in the range of about 5–10°/Ma [*Clarke et al.*, 1998; *Mattei et al.*, 2004], the orientations of fault blocks rotating within a regional velocity field would likewise not change significantly in 10^5 years [see *Roberts and Ganas*, 2000]. It also seems unlikely that the slip rate reorganization was caused by a change in loading associated with erosion/sedimentation/influx of the sea as sea levels are known to have been in the range of zero to −120 m in elevation both before and after 175 ± 75 ka (Figure 5). We suggest that a change in the geometry and size of upper crustal faults through brittle fault growth and interaction is perhaps the only part of the overall Aegean tectonic system that can respond on a 10^5 year timescale, because rates of lateral fault propagation are thought to be at least of the order of tens of millimeters per year (see examples in the work by *Morewood and Roberts* [2002] and discussion by *Walsh et al.* [2002]). Changes in the geometry and size of upper crustal faults through brittle fault growth and interaction may be the dominant control on the slip rate reorganization and localization [*Cowie and Roberts*, 2001].

[57] *Armijo et al.* [1996, 2004] suggested that reorganization of the geometry and size of upper crustal faults in the form of propagation of the strike-slip North Anatolian Fault (Figure 1) was responsible for the high rates of extension in the Gulf of Corinth. However, because localization occurred in the North Sea without the influence of a large strike-slip fault, for the Gulf of Corinth, it may be that reorganization of the geometry of the upper crustal normal fault system solely within central Greece was responsible for the localization. Thus, we are unsure of the role of the North Anatolian Fault and have no data with which to test this hypothesis. Presumably, a dominant role for the propagating North Anatolian Fault would have induced localization in the Gulf of Evia prior to that for the Gulf of Corinth. Thus, a test of whether (1) the 175 ± 75 ka slip rate reorganization occurred on other faults around the Gulf of Corinth and (2) localization occurred earlier in the Gulf of Evia awaits more detailed slip histories for faults with good age control.

8. Conclusions

[58] Measured uplift in the footwall of the fault that ruptured in the 1981 Gulf of Corinth earthquakes (Ms 6.9–6.7) occurs at rates as high as 0.52 mm/yr, decreasing to 0.25 mm/yr over a distance of about 5 km toward the western tip of the fault, constrained by ^{234}U-^{230}Th coral dates associated with deformed paleoshorelines. The spatial change in uplift is caused by a decrease in the slip rate toward the western tip of the fault. Uplift rates, and hence slip rates increased by a factor of 3.2 ± 0.2 at 175 ± 75 ka, constrained by ^{234}U-^{230}Th coral dates, ostracod assemblages and sedimentological observations, synchronous with a cessation of slip on a neighboring fault at 382–112 ka. The increase in slip rate implies that slip on the presently active fault was synchronous with slip on its neighboring normal fault prior to 382–112 ka. We suggest that this is inconsistent with the idea that faults evolved sequentially around the Gulf of Corinth, with active faults initiating to accommodate displacement rates provided by the death of faults located across strike to the south. Instead, we suggest that initial distributed extension occurred on large normal faults located both within the positions of the present-day gulfs of Corinth and Evia and the areas to the south of these gulfs. Acceleration of slip on faults localized extension and vertical motions within the present-day positions of the Gulf of Corinth and Gulf of Evia, associated with a decrease in activity on faults located south and north of the Gulf of Corinth. Such localization of extension within distributed fault systems typifies other rifts such as the Gulf of Suez, the Gulf of California and the North Sea [*Cowie et al.*, 2005]. A test of this synchronous rather than sequential hypothesis for fault activity around the Gulf of Corinth awaits more detailed slip histories for other faults in central Greece. However, the rapid change in fault activity over a period of 0.15 Ma requires the mechanism responsible for localization to have a response time of $\sim 10^5$ years. We suggest that a change in the geometry and size of upper crustal faults through brittle fault growth and interaction is perhaps the only part of the overall Aegean tectonic system that can respond on a 10^5 year timescale and that this may be the dominant control on localization.

[59] **Acknowledgments.** This study was partly funded by NERC grants GR9/01034, GTS/F/90/GS/8, IP/657/0300, IP/787/0902; grants from Birkbeck, UCL Graduate School; the Mineralogical Society of Great Britain and Ireland; and State Scholarship Foundation of Greece (I.K.Y.). We thank IGME (Athens) for permission to conduct field studies in Greece and B. Rosen (Natural History Museum) for identification of *C. caespitosa*. U/Th analyses were carried out at the Uranium Series Facility, Department of Earth Sciences, Open University, Milton Keynes, with XRD carried out

at Birkbeck, University of London, with the help of Steve Hirons. We thank Markos Tranos and Claudio Vita-Finzi for their referee's comments.

References

Abercrombie, R., I. G. Main, A. Douglas, and P. W. Burton (1995), The nucleation and rupture process of the 1981 Gulf of Corinth earthquakes from deconvolved broad-band data, *Geophys. J. Int.*, *120*, 393–405, doi:10.1111/j.1365-246X.1995.tb01827.x.

Ambraseys, N. N., and J. A. Jackson (1990), Seismicity and associated strain of central Greece between 1890 and 1988, *Geophys. J. Int.*, *101*, 663–708, doi:10.1111/j.1365-246X.1990.tb05577.x.

Armijo, R., B. Meyer, G. C. P. King, A. Rigo, and D. Papanastassiou (1996), Quaternary evolution of the Corinth Rift and its implications for the Late Cenozoic evolution of the Aegean, *Geophys. J. Int.*, *126*, 11–53, doi:10.1111/j.1365-246X.1996.tb05264.x.

Armijo, R., F. Flerit, G. King, and B. Meyer (2004), Linear elastic fracture mechanics explains the past and present evolution of the Aegean, *Earth Planet. Sci. Lett.*, *217*, 85–95, doi:10.1016/S0012-821X(03)00590-9.

Bar-Matthews, M., G. J. Wasserburg, and J. H. Chen (1993), Diagenesis of fossil coral skeletons: Correlation between trace elements, texture and $^{234}U/^{238}U$, *Geochim. Cosmochim. Acta*, *57*, 257–276, doi:10.1016/0016-7037(93)90429-Z.

Bell, R. E., L. C. McNeill, J. M. Bull, and T. J. Henstock (2008), Evolution of the offshore western Gulf of Corinth, *Geol. Soc. Am. Bull.*, *120*, 156–178, doi:10.1130/B26212.1.

Billiris, H., et al. (1991), Geodetic determination of tectonic deformation in central Greece from 1900 to 1988, *Nature*, *350*, 124–129, doi:10.1038/350124a0.

Bornovas, J., P. Gaitanakis, and A. Spiridopoulos (1984), Geological map of Greece, Perachora sheet, scale 1:50,000, Inst. of Geol. and Miner. Explor., Athens.

Briole, P., A. Rigo, H. Lyon-Caen, J. C. Ruegg, K. Papazissi, C. Mitsakaki, A. Balodimou, G. Veis, D. Hatzfeld, and A. Deschamps (2000), Active deformation of the Corinth rift, Greece: Results from repeated Global Positioning System surveys between 1990 and 1995, *J. Geophys. Res.*, *105*, 25,605–25,625, doi:10.1029/2000JB900148.

Clarke, P. J., et al. (1998), Crustal strain in central Greece from repeated GPS measurements in the interval 1989–1997, *Geophys. J. Int.*, *135*, 195–214, doi:10.1046/j.1365-246X.1998.00633.x.

Collier, R. E. L., and C. J. Dart (1991), Neogene to Quaternary rifting, sedimentation and uplift in the Corinth Basin, Greece, *J. Geol. Soc.*, *148*, 1049–1065, doi:10.1144/gsjgs.148.6.1049.

Collier, R. E. L., and J. Thompson (1991), Transverse and linear dunes in an upper Pleistocene marine sequence, Corinth Basin, Greece, *Sedimentology*, *38*, 1021–1040, doi:10.1111/j.1365-3091.1991.tb00369.x.

Collier, R. E., M. R. Leeder, P. J. Rowe, and T. C. Atkinson (1992), Rates of tectonic uplift in the Corinth and Megara basins, central Greece, *Tectonics*, *11*, 1159–1167, doi:10.1029/92TC01565.

Collier, R. E. L., D. Pantosti, G. D'Addezio, P. M. De Martini, and E. Masana (1998), Paleoseismicity of the 1981 Corinth earthquake fault: Seismic contribution to extensional strain in central Greece and implications for seismic hazard, *J. Geophys. Res.*, *103*, 30,001–30,019, doi:10.1029/98JB02643.

Collier, R. E. L., M. R. Leeder, M. Trout, G. Ferentinos, E. Lyberis, and G. Papatheodorou (2000), High sedimentary yields and cool, wet winters: Test of last glacial paleoclimates in the northern Mediterranean, *Geology*, *28*, 999–1002, doi:10.1130/0091-7613(2000)28<999:HSYACW>2.0.CO;2.

Cooper, F. J., G. P. Roberts, and C. J. Underwood (2007), A comparison of 10^3–10^5 year uplift rates on the South Alkyonides Fault, central Greece: Holocene climate stability and the formation of coastal notches, *Geophys. Res. Lett.*, *34*, L14310, doi:10.1029/2007GL030673.

Cowie, P. A., and G. P. Roberts (2001), Constraining slip rates and spacings for active normal faults, *J. Struct. Geol.*, *23*, 1901–1915, doi:10.1016/S0191-8141(01)00036-0.

Cowie, P. A., J. R. Underhill, M. D. Behn, J. Lin, and C. E. Gill (2005), Spatio-temporal evolution of strain accumulation derived from multi-scale observations of Late Jurassic rifting in the northern North Sea: A critical test of models for lithospheric extension, *Earth Planet. Sci. Lett.*, *234*, 401–419, doi:10.1016/j.epsl.2005.01.039.

Cowie, P. A., G. P. Roberts, and E. Mortimer (2007), Strain localisation within fault arrays over timescale of 10^0–10^7 years—Observations, explanations and debates, in *Tectonic Faults: Agents of Change on a Dynamic Earth, Dahlem Workshop Report 95*, edited by M. R. Handy, G. Hirth, and N. Hovius, pp. 47–77, MIT Press, Cambridge, Mass.

Davies, R., P. England, B. Parsons, H. Billiris, D. Paradissis, and G. Veis (1997), Geodetic strain of Greece in the interval 1892–1992, *J. Geophys. Res.*, *102*, 24,571–24,588, doi:10.1029/97JB01644.

de Boer, J. Z. (1992), Dilational fractures in the Corinth and Evian rift zones of Greece; their geometrical relations and tectonic significance in the deformational process of normal faulting, *Ann. Tectonicae*, *6*, 41–61.

De Martini, P. M., D. Pantosti, N. Palyvos, F. Lemeille, L. McNeill, and R. Collier (2004), Slip rates of the Aigion and Eliki faults from uplifted marine terraces, Corinth Gulf, Greece, *C. R. Geosci.*, *336*(4–5), 325–334, doi:10.1016/j.crte.2003.12.006.

Dia, A. N., A. S. Cohen, R. K. O'Nions, and J. A. Jackson (1997), Rates of uplift investigated through ^{230}Th dating in the Gulf of Corinth (Greece), *Chem. Geol.*, *138*, 171–184, doi:10.1016/S0009-2541(97)00010-7.

Doutsos, T., and G. Poulimenos (1992), The geometry and kinematics of active faults and their seismotectonic significance in the western Corinth-Patras rift, (Greece), *J. Struct. Geol.*, *14*, 689–700, doi:10.1016/0191-8141(92)90126-H.

Edwards, L. E., J. H. Chen, and G. J. Wasserburg (1987), ^{238}U-^{234}U-^{230}Th-^{232}Th systematics and the precise measurement of time over the past 500,000 years, *Earth Planet. Sci. Lett.*, *81*, 175–192, doi:10.1016/0012-821X(87)90154-3.

Flotté, N., V. Plagnes, D. Sorel, and A. Benedicto (2001), Attempt to date Pleistocene normal faults of the Corinth-Patras Rift (Greece) by U/Th method, and tectonic implications, *Geophys. Res. Lett.*, *28*, 3769–3772, doi:10.1029/2001GL012964.

Goldsworthy, M., and J. Jackson (2001), Migration of activity within normal fault systems: Examples from the Quaternary mainland of Greece, *J. Struct. Geol.*, *23*, 489–506, doi:10.1016/S0191-8141(00)00121-8.

Goldsworthy, M., J. Jackson, and J. Haines (2002), The continuity of active fault systems in Greece, *Geophys. J. Int.*, *148*(3), 596–618, doi:10.1046/j.1365-246X.2002.01609.x.

Gupta, S., P. A. Cowie, N. H. Dawers, and J. R. U. Underhill (1998), A mechanism to explain rift-basin subsidence and stratigraphic patterns through fault array evolution, *Geology*, *26*, 595–598, doi:10.1130/0091-7613(1998)026<0595:AMTERB>2.3.CO;2.

Hearty, P. J., J. T. Hollin, A. Conrad Neumann, M. J. O'Leary, and M. McCulloch (2007), Global sea-level fluctuations during the Last Interglaciation (MIS 5e), *Quat. Sci. Rev.*, *26*, 2090–2112, doi:10.1016/j.quascirev.2007.06.019.

Higgs, B. (1988), Syn-sedimentary structural controls on basin deformation in the Gulf of Corinth, Greece, *Basin Res.*, *1*, 155–165.

Houghton, S. L., G. P. Roberts, I. D. Papanikolaou, J. M. McArthur, and M. A. Gilmour (2003), New ^{234}U-^{230}Th coral dates from the western Gulf of Corinth: Implications for extensional tectonics, *Geophys. Res. Lett.*, *30*(19), 2013, doi:10.1029/2003GL018112.

Hubert, A., G. C. P. King, R. Armijo, B. Meyer, and D. Papanastassiou (1996), Fault reactivation, stress interaction and rupture propagation in the 1981 Corinth earthquake sequence, *Earth Planet. Sci. Lett.*, *142*, 573–585, doi:10.1016/0012-821X(96)00108-2.

Jackson, J. (1999), Fault death: A perspective from actively deforming areas, *J. Struct. Geol.*, *21*, 1003–1010, doi:10.1016/S0191-8141(99)00013-9.

Jackson, J. A., J. Gagnepain, G. Houseman, G. C. P. King, P. Papadimitriou, C. Soufleris, and J. Virieux (1982), Seismicity, normal faulting, and the geomorphological development of the Gulf of Corinth (Greece): The Corinth earthquakes of February and March 1981, *Earth Planet. Sci. Lett.*, *57*, 377–397, doi:10.1016/0012-821X(82)90158-3.

Jouzel, J., et al. (2007), Orbital and millennial Antarctic climate variability over the past 800,000 years, *Science*, *317*, 793–796, doi:10.1126/science.1141038.

Keraudren, B., and D. Sorel (1987), The terraces of Corinth (Greece)—A detailed record of eustatic sea-level variations during the last 500,000 years, *Mar. Geol.*, *77*, 99–107, doi:10.1016/0025-3227(87)90085-5.

Kershaw, S., and L. Guo (2001), Marine notches in coastal cliffs; indicators of relative sea-level change, Perachora Peninsula, central Greece, *Mar. Geol.*, *179*, 213–228, doi:10.1016/S0025-3227(01)00218-3.

Kostrov, V. (1974), Seismic moment and energy of earthquakes, and seismic flow of rock, *Izv. Acad. Sci. USSR Phys. Solid Earth*, Engl. Transl., *1*, 23–44.

Leeder, M. R., L. C. McNeill, R. E. L. Collier, C. Portman, P. J. Rowe, J. E. Andrews, and R. L. Gawthorpe (2003), Corinth rift margin uplift: New evidence from Late Quaternary marine shorelines, *Geophys. Res. Lett.*, *30*(12), 1611, doi:10.1029/2003GL017382.

Leeder, M. R., C. Portman, J. E. Andrews, R. E. L. Collier, E. Finch, R. L. Gawthorpe, L. C. McNeill, M. Pérez-Arlucea, and P. Rowe (2005), Normal faulting and crustal deformation, Alkyonides Gulf and Perachora peninsula, eastern Gulf of Corinth rift, Greece, *J. Geol. Soc.*, *162*(3), 549–561, doi:10.1144/0016-764904-075.

Malartre, F., M. Ford, and E. A. Williams (2004), Preliminary biostratigraphy and 3D geometry of the Vouraikos Gilbert-type fan delta, Gulf of Corinth, Greece, *C. R. Geosci.*, *336*(4–5), 269–280, doi:10.1016/j.crte.2003.11.016.

Mariolakos, I., and S. C. Stiros (1987), Quaternary deformation of the Isthmus and Gulf of Corinthos (Greece), *Geology*, *15*, 225–228, doi:10.1130/0091-7613(1987)15<225:QDOTIA>2.0.CO;2.

Mattei, M., N. D'Agostino, I. Zananiri, D. Kondopoulou, S. Pavlides, and V. Spatharas (2004), Tectonic evolution of fault-bounded continental blocks: Comparison of paleomagnetic and GPS data in the Corinth and Megara basins (Greece), *J. Geophys. Res.*, *109*, B02106, doi:10.1029/2003JB002506.

McNeill, L. C., and R. E. Collier (2004), Ll., Uplift and slip rates of the eastern Eliki fault segment, Gulf of Corinth, Greece, inferred from Holocene and Pleistocene terraces, *J. Geol. Soc.*, *161*, 81–92, doi:10.1144/0016-764903-029.

McNeill, L. C., C. J. Cotterill, T. J. Henstock, J. M. Bull, A. Stefatos, R. E. L. Collier, G. Papatheoderou, G. Ferentinos, and S. E. Hicks (2005), Active faulting within the offshore western Gulf of Corinth, Greece: Implications for models of continental rift deformation, *Geology*, *33*(4), 241–244, doi:10.1130/G21127.1.

Morewood, N. C., and G. P. Roberts (1997), The geometry, kinematics and rates of deformation in a normal fault segment boundary, central Greece, *Geophys. Res. Lett.*, *24*, 3081–3084, doi:10.1029/97GL03100.

Morewood, N. C., and G. P. Roberts (1999), Lateral propagation of the surface trace of the South Alkyonides fault, central Greece: Its impact on models of fault growth and displacement-length relationships, *J. Struct. Geol.*, *21*, 635–652, doi:10.1016/S0191-8141(99)00049-8.

Morewood, N. C., and G. P. Roberts (2001), Comparison of surface slip and focal mechanism data along normal faults: An example from the eastern Gulf of Corinth, Greece, *J. Struct. Geol.*, *23*, 473–487, doi:10.1016/S0191-8141(00)00126-7.

Morewood, N. C., and G. P. Roberts (2002), Surface observations of active normal fault propagation: Implications for growth, *J. Geol. Soc.*, *159*, 263–272, doi:10.1144/0016-764901-046.

Ori, G. G. (1989), Geologic history of the extensional basin of the Gulf of Corinth (?Miocene-Pleistocene), Greece, *Geology*, *17*(10), 918–921, doi:10.1130/0091-7613(1989)017<0918:GHOTEB>2.3.CO;2.

Pantosti, D., R. Collier, G. D'Addezio, E. Masana, and D. Sakellariou (1996), Direct geological evidence for prior earthquakes on the 1981 Corinth fault (central Greece), *Geophys. Res. Lett.*, *23*, 3795–3798, doi:10.1029/96GL03647.

Perissoratis, C., D. J. W. Piper, and V. Lykousis (2000), Alternating marine and lacustrine sedimentation during late Quaternary in the Gulf of Corinth rift basin, central Greece, *Mar. Geol.*, *167*, 391–411, doi:10.1016/S0025-3227(00)00038-4.

Pirazzoli, P. A., S. C. Stiros, M. Arnold, J. Laborel, F. Laborel-Deguen, and S. Papageorgiou (1994), Episodic uplift deduced from Holocene shorelines in the Perachora Peninsula, Corinth area, Greece, *Tectonophysics*, *229*, 201–209, doi:10.1016/0040-1951(94)90029-9.

Portman, C., J. E. Andrews, P. J. Rowe, M. R. Leeder, and J. Hoogewerff (2005), Submarine-spring controlled calcification and growth of large Rivularia bioherms, late Pleistocene (MIS 5e), Gulf of Corinth, Greece, *Sedimentology*, *52*, 441–465, doi:10.1111/j.1365-3091.2005.00704.x.

Roberts, G. P. (1996a), Variation in fault-slip directions along active and segmented normal fault systems, *J. Struct. Geol.*, *18*, 835–845, doi:10.1016/S0191-8141(96)80016-2.

Roberts, G. P. (1996b), Noncharacteristic normal faulting surface ruptures from the Gulf of Corinth, Greece, *J. Geophys. Res.*, *101*, 25,255–25,267, doi:10.1029/96JB02119.

Roberts, G. P., and I. S. Stewart (1994), Uplift, deformation and fluid involvement within an active normal fault zone in the Gulf of Corinth, Greece, *J. Geol. Soc.*, *151*, 531–542, doi:10.1144/gsjgs.151.3.0531.

Roberts, S., and J. A. Jackson (1991), Active normal faulting in central Greece: An overview, in *The Geometry of Normal Faults*, edited by A. M. Roberts, G. Yielding, and B. Freeman, *Geol. Soc. Spec. Publ.*, *56*, 125–142, doi:10.1144/GSL.SP.1991.056.01.09.

Sakellariou, D., V. Lykousis, S. Alexandri, H. Kaberi, G. Rousakis, P. Nomikou, P. Georgiou, and D. Ballas (2007), Faulting, seismic-stratigraphic architecture and late Quaternary evolution of the Gulf of Alkyonides Basin–east Gulf of Corinth, central Greece, *Basin Res.*, *19*, 273–295, doi:10.1111/j.1365-2117.2007.00322.x.

Siddall, M., E. J. Rohling, A. Almogi-Labin, C. Hemleben, D. Meischner, I. Schmelzer, and D. A. Smeed (2003), Sea-level fluctuations during the last glacial cycle, *Nature*, *423*, 853–858, doi:10.1038/nature01690.

Stefatos, A., G. Papatheodorou, G. Ferentinos, M. Leeder, and R. Collier (2002), Seismic reflection imaging of active offshore faults in the Gulf of Corinth: Their seismotectonic significance, *Basin Res.*, *14*, 487–502, doi:10.1046/j.1365-2117.2002.00176.x.

Stein, M., G. J. Wasserburg, P. Aharon, J. H. Chen, Z. R. Zhu, A. Bloom, and J. Chappell (1993), TIMS U-series dating and stable isotopes of the last interglacial event in Papua New Guinea, *Geochim. Cosmochim. Acta*, *57*, 2541–2554, doi:10.1016/0016-7037(93)90416-T.

Stein, R. S., and S. E. Barrientos (1985), Planar high-angle faulting in the Basin and Range: Geodetic analysis of the 1983 Borah Peak, Idaho, earthquake, *J. Geophys. Res.*, *90*, 11,355–11,366, doi:10.1029/JB090iB13p11355.

Stewart, I., and C. Vita-Finzi (1996), Coastal uplift on active normal faults; the Eliki Fault, Greece, *Geophys. Res. Lett.*, *23*, 1853–1856, doi:10.1029/96GL01595.

Stirling, C., T. M. Esat, M. T. McCulloch, and K. Lambeck (1995), High-precision U-series dating of corals from Western Australia and implications for the timing and duration of the Last Interglacial, *Earth Planet. Sci. Lett.*, *135*, 115–130, doi:10.1016/0012-821X(95)00152-3.

Taymaz, T., J. A. Jackson, and D. P. McKenzie (1991), Active tectonics of the north and central Aegean, *Geophys. J. Int.*, *106*, 433–490, doi:10.1111/j.1365-246X.1991.tb03906.x.

Turner, J., M. Leeder, J. Andrews, and P. Rowe (2008), Comment on "A comparison of 10^3–10^5 year uplift rates on the South Alkyonides Fault, central Greece: Holocene climate stability and the formation of coastal notches" by J. F. Cooper, G. P. Roberts, and C. J. Underwood, *Geophys. Res. Lett.*, *35*, L19314, doi:10.1029/2008GL034854.

van Calsteren, P., and J. B. Schwieters (1995), Performance of a thermal ionization mass-spectrometer with a deceleration lens system and post-deceleration detector selection, *Int. J. Mass Spectrom. Ion Processes*, *146–147*, 119–129, doi:10.1016/0168-1176(95)04208-3.

van Calsteren, P., and L. E. Thomas (2006), Uranium-series dating applications in natural environmental science, *Earth Sci. Rev.*, *75*, 155–175, doi:10.1016/j.earscirev.2005.09.001.

Vita-Finzi, C. (1993), Evaluating late Quaternary uplift in Greece and Cyprus, in *Magmatic Processes and Plate Tectonics*, edited by H. M. Prichard et al., *Geol. Soc. Spec. Publ.*, *76*, 417–424, doi:10.1144/GSL.SP.1993.076.01.21.

Vita-Finzi, C., and G. C. P. King (1985), The seismicity, geomorphology and structural evolution of the Corinth area of Greece, *Philos. Trans. R. Soc. London, Ser. A*, *314*, 379–407, doi:10.1098/rsta.1985.0024.

Walsh, J. J., A. Nicol, and C. Childs (2002), An alternative model for the growth of faults, *J. Struct. Geol.*, *24*, 1669–1675, doi:10.1016/S0191-8141(01)00165-1.

Westaway, R. (1996), Quaternary elevation change in the Gulf of Corinth of central Greece, *Philos. Trans. R. Soc. London, Ser. A*, *354*, 1125–1164, doi:10.1098/rsta.1996.0043.

Westaway, R. (1998), Dependence of active normal fault dips on lower-crustal low regimes, *J. Geol. Soc.*, *155*, 233–253, doi:10.1144/gsjgs.155.2.0233.

Westaway, R. (2002), The Quaternary evolution of the Gulf of Corinth, central Greece: Coupling between surface processes and flow in the lower continental crust, *Tectonophysics*, *348*, 269–318, doi:10.1016/S0040-1951(02)00032-X.

Westaway, R. (2007), Improved modelling of the Quaternary evolution of the Gulf of Corinth, incorporating erosion and sedimentation coupled by lower-crustal flow, *Tectonophysics*, *440*, 67–84, doi:10.1016/j.tecto.2007.02.002.

F. J. Cooper, School of Earth and Space Exploration, Arizona State University, Tempe, AZ 85287, USA.

P. A. Cowie, Institute of Earth Science, School of GeoSciences, Edinburgh University, Edinburgh EH8 9XP, UK.

S. L. Houghton, J. M. McArthur, I. Papanikolaou, G. P. Roberts, C. Underwood, and T. Wigley, Research School of Earth Sciences, UCL/Birkbeck, University of London, Gower Street, London WC1E 6BT, UK.

P. van Calsteren, Uranium Series Facility, Department of Earth Sciences, Open University, Milton Keynes MK7 6BJ, UK.